ACS APPLIED MATERIALS & INTERFACES

Review

Cite This: ACS Appl. Mater. Interfaces 2018, 10, 21035−21055

www.acsami.org

Graphitic Carbon Nitride-Based Heterojunction Photoactive Nanocomposites: Applications and Mechanism Insight

Danlian Huang,*[,†,‡] Xuelei Yan,[†,‡] Ming Yan,*[,†,‡] Guangming Zeng,[†,‡] Chengyun Zhou,[†,‡] Jia Wan,[†,‡] Min Cheng,[†,‡] and Wenjing Xue[†,‡]

[†]College of Environmental Science and Engineering, Hunan University, Changsha, Hunan 410082, China

[‡]Key Laboratory of Environmental Biology and Pollution Control, Hunan University, Ministry of Education, Changsha, Hunan 410082, China

ABSTRACT: The design of heterojunction with superior performance of light absorption and appropriate conduction band and valence band potentials is a promising approach for the applications in efficient environmental remediation and the solar energy storage. In recent years, many studies have been devoted to the applications of graphitic carbon nitride (g-C_3N_4)-based heterojunction photoactive nanomaterials under visible light irradiation due to its excellent physical, optical, and electrical properties, which inspired us to compile this review. Although many reviews demonstrated about the syntheses and applications of g-C_3N_4 composites, a targeted review on the systematic application and photocatalytic mechanisms of g-C_3N_4-based heterojunction, in which components are in intimate linkage with each other rather than a physical mixture, is still absent. In this review, the applications of g-C_3N_4-based heterojunction photoactive nanomaterials in environmental remediation and solar energy storage, such as photocatalytic treatment of persistent organic pollutants, heavy-metal-ion redox, oxidative decomposition of pathogens, water splitting for H_2 evolution, and CO_2 reduction, are systematically discussed. In addition, some emerging applications, such as solar cells and biosensors, are also introduced. Meanwhile, a comprehensive assessment on the basis of first-principles calculations and the thermodynamics and kinetics of surface catalytic reaction for the electronic structure and photocatalytic properties of g-C_3N_4-based heterojunction are valued by this review. In the end, a brief summary and perspectives in designing practical heterojunction photoactive nanomaterials also showed the bright future of g-C_3N_4-based heterojunction. Altogether, this review systematically complements the information that previous reviews have frequently ignored and points out the future development trends of g-C_3N_4-based heterojunction, which expected to provide important references and right directions for the development and practical applications of g-C_3N_4-based heterojunction photoactive nanomaterials.

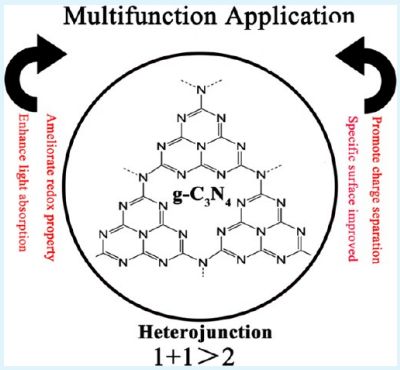

KEYWORDS: *g-C_3N_4, heterojunction, photocatalysis, mechanism, application*

1. INTRODUCTION

In the last few decades, environmental problems, such as organic pollutants, heavy-metal pollution, pathogenic microorganisms, and energy shortage, have posed severe threats to the sustainable development of humans.[1] To solve more and more serious problems, semiconductor-based photocatalysis offers a "green" and sustainable technology for environmental remediation and energy storage by the utilization of solar light energy.[2] Since the 1970s, domestic and foreign scholars have done a lot of research works on many aspects of semiconductor photocatalysis and have made certain achievements in many fields. Especially, in 1972, Fujishima and Honda found that titanium dioxide (TiO_2) is an excellent photocatalyst.[3] Then, Carey et al. found the photodegradation ability of TiO_2 toward organic pollutants in aqueous solution, which opened the gate of TiO_2 photocatalysis in the field of the environment.[4] Currently, TiO_2 has become the best-studied photocatalyst with excellent ultraviolet (UV) light activity.[5,6] Unfortunately, because of the wide band gap (3.2 eV), the light response region of TiO_2 is relatively narrow, which greatly limits the solar energy utilization efficiency of TiO_2 because the energy distribution of solar energy is less than 5% for UV light.[7] To tackle this problem, visible light-driven photocatalysts have drawn the attention of researchers in recent years.[8] Graphitic carbon nitride (g-C_3N_4) has been focused by various scientific researchers thanks to its graphene-like structure, mild band gap (2.7 eV), good visible light (VL) absorption, excellent thermal and chemical stabilities, and nonmetal and photocatalytic properties.[9]

As early as 1834, C_3N_4 named as "melon" was reported to be one of the oldest synthetic polymers.[10] In 1940, Redemann and Lucas found that "melon" has a stable graphite structure.[11] It was not until 2009 that g-C_3N_4 was reported as a photocatalyst by Wang et al.[12] Over the past few years, as a two-dimensional-conjugated polymeric photocatalyst, g-C_3N_4 has made great progress in various applications of environment remediation

Received: March 3, 2018
Accepted: June 1, 2018
Published: June 1, 2018

DOI: 10.1021/acsami.8b03620
ACS Appl. Mater. Interfaces 2018, 10, 21035−21055

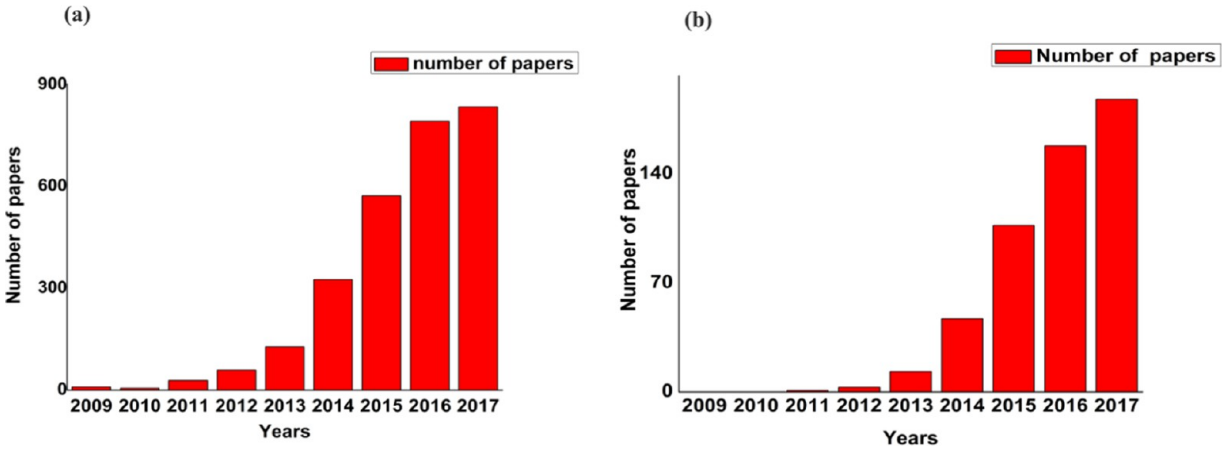

Figure 1. Year-by-year publications on (a) g-C_3N_4 an (b) GBHs (data from the Web of Science).

and energy storage. Above all, g-C_3N_4 is easily synthesized by thermal polymerization of abundant nitrogen-rich precursors, such as urea,[13] melamine,[14] dicyandiamide,[15] cyanamide,[16] thiourea,[17] and ammonium thiocyanate,[18] which provides a great possibility for practical applications of g-C_3N_4. Meanwhile, the results of thermogravimetric analysis showed that the thermal stability of g-C_3N_4 is excellent up to ca. 600 °C in air.[19] Beyond that, g-C_3N_4 exhibits an outstanding chemical stability.[20] However, several obstacles and shortcomings of pure g-C_3N_4, such as low electrical conductivity, high recombination ratio of photoinduced carriers, and the absence of light absorption above 460 nm, have been discovered by in-depth research.[21,22]

To date, many modification methods were applied to promote the photocatalytic activity of pure g-C_3N_4. For example, increasing the surface area of g-C_3N_4 can increase the number of active facets, improving the photocatalytic efficiency. By controlling the growth process of g-C_3N_4 nanoparticles, nanostructured g-C_3N_4 with large specific surface area can be prepared, which can improve the photocatalytic efficiency significantly.[23,24] Foreign elements, such as boron and nitrogen, can be introduced into the structural framework of graphite, leading to tunable electric properties from highly conductive (graphene) to semiconducting (BCN and C_3N_4).[25,26] To narrow the band gap, Yan et al. introduced boron into g-C_3N_4, thereby improving the utilization efficiency of solar energy.[27] Although g-C_3N_4 prepared by the above method shows excellent photocatalytic properties, it still has a series of limitations. For instance, a high ratio of active surface area can be achieved by controlling the exposed facets of the semiconductor, whereas the well-crystallized nanoparticles are generally larger than granular nanoparticles and the amount of active surface of per unit mass did not increase.[28]

Actually, among various modification routes, g-C_3N_4 integrated with other substances, such as noble metals and other semiconductors, to form heterojunction is regarded as a reliable and effective way to enhance its properties, which could obtain unique nanostructures to increase the separation rate of photogenerated carriers and to utilize a wider spectrum of sunlight. In general, the heterojunctions should have appropriate band positions of the two substances for the energy-level offsets, which leads to the accumulation of space charge at the interfaces of the two components for facilitating the separation of photogenerated carriers. Because of their excellent physical, optical, and electrical properties, extensive g-C_3N_4-based heterojunction (GBH) nanocomposites have been applied to solve multifarious environmental pollution and energy shortage under visible light irradiation. Many interesting findings about GBH photoactive nanomaterials have been reported extensively. As shown in Figure 1, more than 2500 papers about g-C_3N_4 have been published since 2009, of which more than 500 papers report on GBH and show an increasing trend every year.

So far, some exciting reviews on g-C_3N_4-based composite photocatalysts about their synthesis techniques, characteristic features, and promising applications have been reported.[29,30] Nevertheless, according to current information, there are few review articles that have systematic exposition of the latest applications of GBH, as well as the critical roles of the heterojunction in promoting the photocatalytic performance. Therefore, a comprehensive and critical review about the mechanisms and the latest applications of GBH photoactive nanomaterials is necessary to provide important references and right directions for further advances of GBH from the viewpoint of practical application. In addition, some emerging applications, such as solar cells and biosensors, have been neglected frequently by previous reviews, which are important sections of GBH systems in solar energy conversion and sensor development.

In this review, the latest reports on the applications of the GBH, such as photocatalytic treatment of persistent organic pollutants (POPs), heavy-metal-ion redox and pathogen oxidative decomposition, water splitting for H_2 evolution, and CO_2 reduction will be systematically discussed. Furthermore, some emerging applications, such as solar cells and biosensors, are also introduced. In addition to the description of multifunctional applications of GBH, the potential mechanisms of GBH based on charge transfer, first-principles calculations, and the thermodynamics and kinetics of surface catalytic reaction will also be emphasized and elaborated.

Altogether, this review systematically complements the information that previous reviews have frequently ignored and points out the future development trends of GBH, which promote the design of GBH for target-specific applications. It is predictable that a lot of undiscovered potentiality is still present on GBH photoactive nanocomposites for researchers to explore.

DOI: 10.1021/acsami.8b03620
ACS Appl. Mater. Interfaces 2018, 10, 21035−21055

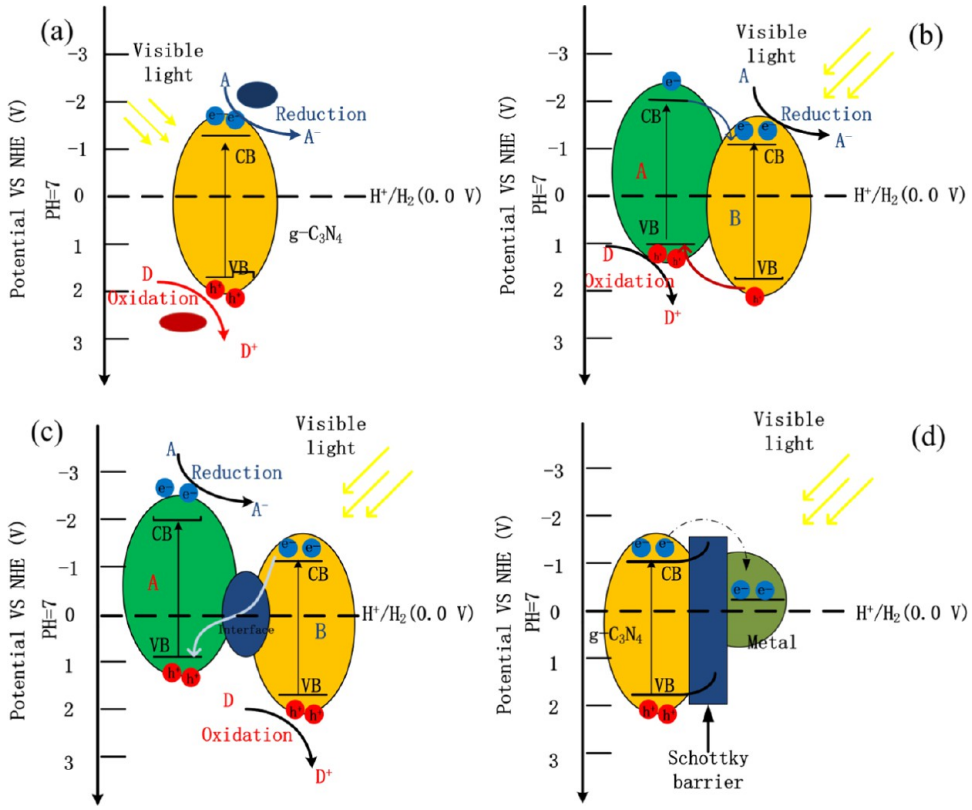

Figure 2. (a) Photocatalytic mechanism of pure g-C_3N_4; schematic illustration of the transfer of photoinduced carriers for various types of heterojunction nanocomposites; (b) type II heterojunction; (c) Z-scheme heterojunction; and (d) Schottky junction.

2. APPLICATIONS OF G-C_3N_4-BASED HETEROJUNCTION IN ENVIRONMENT REMEDIATION

2.1. Photocatalytic Mechanisms of g-C_3N_4-Based Heterojunction. *2.1.1. Photoinduced Charge-Transfer Mechanisms of g-C_3N_4-Based Heterojunction.* Different from metals, the energy band of semiconductors is discontinuous and a band gap exists between the valence band (VB) and the conduction band (CB). When a semiconductor located at the ground state, its chemical stability is outstanding. As shown in Figure 2a, when g-C_3N_4 is irradiated with photons, whose energy is no less than the band gap energy of g-C_3N_4, the electrons get excited and then jump to the CB, producing corresponding holes on the VB. Then, the photoinduced electron−hole pairs can be segregated and moved to the semiconductor surface under the control of an electric field, resulting in highly active electrons and holes on the surface of the semiconductor. The electrons in the CB with a chemical potential of +0.5 to −1.5 V (vs normal hydrogen electrode (NHE)) and holes in the VB with a chemical potential of +1.0 to +3.5 V (vs NHE) reveal excellent reduction and oxidation abilities, respectively.[31] Therefore, electrons and holes can be used as a reductant and oxidant to react with electron acceptors and donors attached to the surface of the semiconductor, respectively. However, the photogenerated electrons and holes may also be directly combined in the interior or surface of photocatalyst and disperse the input energy in terms of heat or emitted light, resulting in a decrease of the utilization rate of photoinduced carriers for desired photoreactions.

For the sake of improving the photocatalytic ability, the separation process of electron−hole pairs should be effective and photoinduced carriers should be rapidly transferred across the surface/interface to inhibit the recombination. The universally applicable method is the formation of heterojunction by coupling with other substances. When g-C_3N_4 makes contact with other semiconductors, band bending occurs at the interface and leads to the formation of in-built electric field (IEF). Therefore, the separation rate of photogenerated electron−hole pairs is greatly increased in well-designed GBH in the presence of an IEF.

According to the charge-transfer mechanisms, the frequently reported GBHs in the existing research can be mainly divided into two categories: type II heterojunction system and Z-scheme heterojunction system. The type II heterojunction system is a widely used type at present. As shown in Figure 2b, the band edge potentials of type II heterojunction are staggered between semiconductor A and semiconductor B. Under sunlight irradiation, photogenerated electrons move from the CB of semiconductor A to the CB of semiconductor B and holes transfer to the VB of semiconductor A from the VB of semiconductor B, which make the photogenerated electrons and holes enriched in two semiconductors, respectively. Moreover, the rates of oxidation and reduction reactions increased due to the space separation where the reactions take place. In addition, it not only increases the number of electrons and holes in the reduction and oxidation reactions, but also forms space separation of the photogenerated carriers, inhibiting the recombination of electron−hole pairs.

However, because the photogenerated electrons and holes shift to the less negative CB and the less positive VB, respectively, the redox abilities of electrons and holes in type II

DOI: 10.1021/acsami.8b03620
ACS Appl. Mater. Interfaces 2018, 10, 21035−21055

heterojunction system are weakened. To solve the aforementioned problems, a novel heterojunction charge-transfer scheme is proposed, which is named as Z-scheme heterojunction.[32] The photogenerated electrons on the CB of semiconductor B can be combined with the photogenerated holes on the VB of semiconductor A due to the transmission of interface phase in Z-scheme heterojunction system (Figure 2c). Although the number of photogenerated carriers involved in the reaction is reduced, the photogenerated electrons and holes can be enriched with more negative CB potential and more positive VB potential, indicating higher redox ability. In recent years, some studies have been reported about switching of type II heterojunction to direct Z-scheme heterojunction via modulating the interfacial band bending, which offers a good thinking about the construction of high-performance Z-scheme heterojunction system.[33]

In addition, the Schottky junctions formed by g-C_3N_4 and metals are also important components of GBH systems. Under sunlight irradiation, g-C_3N_4 could be excited and resulting electrons migrate from the higher Fermi levels of g-C_3N_4 to metal until the two levels match (Figure 2d). Metal particles can improve charge separation at the interface of the metal−semiconductor heterojunction, which in turn contributes to an enhancement in the catalytic properties.[34] Moreover, g-C_3N_4 not only acts as a support, but can also confine the aggregation of the metal particles, further promoting the selectivity and activity.[35] The Schottky barrier and space charge region were formed at the interface between metal and g-C_3N_4 because of the different Fermi levels and work functions of metal and g-C_3N_4 when they were in close contact. The Schottky junctions with rectifying characteristics and lower interface voltage can modulate the generation and flow of photogenerated electrons and separate electron−hole pairs more effectively.[36] Meanwhile, the surface plasmon resonance of metal nanoparticles is a key factor to increase the photocatalytic performance of GBH. Obviously, there will be a good prospect in the future of GBH in redox reactions according to these mechanisms.

2.1.2. Origin of Excellent Photocatalytic Properties in g-C_3N_4-Based Heterojunction on the Basis of Theoretical Calculation. Recently, with the extensive study of the applications of GBH, more attention has been paid to the research on the microelectronic structure and photocatalytic reaction mechanism of GBH on the basis of first-principles calculations, which provided an important reference value for the practical applications of GBH.

In the research conducted by Liang et al.,[37] the first-principles calculation was used to studied the photocatalytic performances and electronic structure of layered g-C_6N_6/g-C_3N_4 heterojunction. The calculation results of density of states (DOS) and band structure demonstrated that the g-C_6N_6/g-C_3N_4 heterojunction possessed an indirect band gap. Moreover, the valence band maximum (VBM) of the g-C_6N_6/g-C_3N_4 heterojunction became more delocalized, which indicated that the mobility of photogenerated holes can be significantly improved. In addition, the g-C_6N_6/g-C_3N_4 heterojunction had a narrower band gap than pure g-C_3N_4, which means a wider range of absorbance. Liu found that the band edge positions of g-C_3N_4 and CdS changed after g-C_3N_4 and CdS contact closely according to the hybrid density functional theory (DFT) approach.[38] DOS, charge density difference, and Bader charge analysis showed that the internal electric field could further diminish the electron−hole pair recombination. Meanwhile, the VBM and CBM of g-C_3N_4/CdS (110) heterojunction are located at Γ point and M point, respectively, which indicated an indirect gap (2.02 eV). Using the first-principles calculations, Zhang et al. found that the ZrS_2/g-C_3N_4 heterojunction had suitable CBM and VBM positions with efficient charge separation and excellent light absorption under visible light.[39] The charge redistribution is mainly created at the interface region of the hybrid ZrS_2/g-C_3N_4 heterostructure. The internal polarized field plays an important role on photocatalytic performance enhancement. According to DFT calculation, Gao et al. found that type II van der Waals heterojunction was formed between g-C_3N_4 and trigonal/hexagonal-shaped carbon nanodots (C-dots), which led to the significant narrowing of the band gap.[40] In addition, the band alignment calculation results based on the hybrid functional method showed that C-dots could function as a photosensitizer in C-dots/g-C_3N_4 system for promoting photocatalytic activity.

In summary, the first-principles calculations based on DFT of GBH showed that the formation of heterojunction led to a significant reduction of band gap as well as enhancement of photoinduced electron−hole pairs separation and visible light response, resulting in excellent properties in GBH. Meanwhile, these studies demonstrated that the GBH would be a promising tool in multifunction applications.

2.1.3. Thermodynamics and Kinetics of Surface Catalytic Reactions Based on g-C_3N_4-Based Heterojunction. 2.1.3.1. Thermodynamics. In various GBH photocatalytic systems, problems such as high recombination rate and low utilization of solar energy have been solved. However, appropriate CB and VB positions were also essential for an excellent GBH photocatalytic system. From the thermodynamic viewpoint, surface catalytic reactions could be driven by the electrons and holes when the oxidation−reduction potential is located between the CB and VB potentials. For example, to realize overall water splitting, the VB potential of semiconductor must be more positive than that of O_2 generation and its CB potential must be more negative than that of H_2 generation. In several types of GBH summarized in this article, Z-scheme heterojunctions showed stronger redox ability due to their special charge-transfer mechanism. Theoretically, the wider band gap of heterojunction systems indicated the stronger ability of driving redox reaction. But in another aspect, the wider band gap also means a narrower optical absorption region. Therefore, the obvious contradiction between the redox abilities and absorption capacity of visible light should be carefully optimized and balanced in the development of well-designed GBH photocatalytic systems.

2.1.3.2. Kinetics. In general, the photocatalytic reactivity depends on the thermodynamic and kinetic equilibrium of the following three processes: light absorption, generation and separation of the photogenerated carriers, and surface catalytic reaction.[41] Obviously, the reduction of efficiency at each stage will affect the overall photocatalytic efficiency. In GBH systems, the light absorption ability and photogenerated carrier generation and separation have been greatly enhanced by the effect of IEF and appropriate CB and VB positions, which functioned as an effective approach to accelerate the surface reaction kinetics. In addition, specific surface area of photocatalyst is an important factor for the kinetics of surface catalytic reactions. The low specific surface area means not only less active sites but also more mass-transport barriers of the adsorbed species, both of which may reduce the efficiency of the photocatalyst.[42,43] Meanwhile, low specific surface area will also cause accumulation of photogenerated electrons and holes

DOI: 10.1021/acsami.8b03620
ACS Appl. Mater. Interfaces 2018, 10, 21035−21055

Table 1. Degradation of POPs by g-C_3N_4-Based Heterojunctions

photocatalysts	type of heterojunctions	applications	ref (year)
TiO_2/g-C_3N_4	type II	degradation of methyl orange (MO) and phenol	49 (2015)
$AgVO_3$/g-C_3N_4	type II	degradation of fuchsin and bisphenol A (BPA)	50 (2015)
AgI/g-C_3N_4	type II	degradation of MO and 4-chlorophenol (4-CP)	51 (2013)
$Bi_2O_2CO_3$/g-C_3N_4	type II	degradation of rhodamine B (RhB) and phenol	52 (2014)
$Bi_5Nb_3O_{15}$/g-C_3N_4	type II	degradation of MO and 4-chlorophenol	53 (2013)
CuTCPP/g-C_3N_4	type II	degradation of phenol	54 (2015)
SnS_2/g-C_3N_4	type II	degradation of RhB, methyl orange, and 4-nitrophenol	55 (2015)
Sb-doped SnO_2/ g-C_3N_4	type II	CO_2 reduction and gaseous isopropyl alcohol (IPA) oxidation	56 (2018)
g-C_3N_4/BiOI	type II	degradation of 4-CP BPA	56 (2014)
V_2O_5/g-C_3N_4	Z-scheme	degradation of RhB and tetracycline	57 (2016)
$Bi_{20}TiO_{32}$/g-C_3N_4	Z-scheme	degradation of RhB and 4-chlorophenol	58 (2015)
g-C_3N_4/BiOI	Z-scheme	degradation of microcystin-LR	59 (2017)
Co_3O_4/g-C_3N_4	Z-scheme	degradation of tetracycline hydrochloride	60 (2018)
g-C_3N_4/carbon nanotube (CNT)/Bi_2WO_6	Z-scheme	degradation of tetracycline hydrochloride	61 (2018)
g-C_3N_4/MnO_2	Z-scheme	degradation of dye and phenol	62 (2018)
g-C_3N_4/Bi_4O_7	Z-scheme	degradation MB, phenol, RhB, and BPA	63 (2017)
g-C_3N_4/OD-ZnO	Z-scheme	degradation of 4-chlorophenol and H_2 evolution	64 (2017)
Ag_3PO_4/g-C_3N_4	Z-scheme	degradation of sulfamethoxazole	65 (2017)

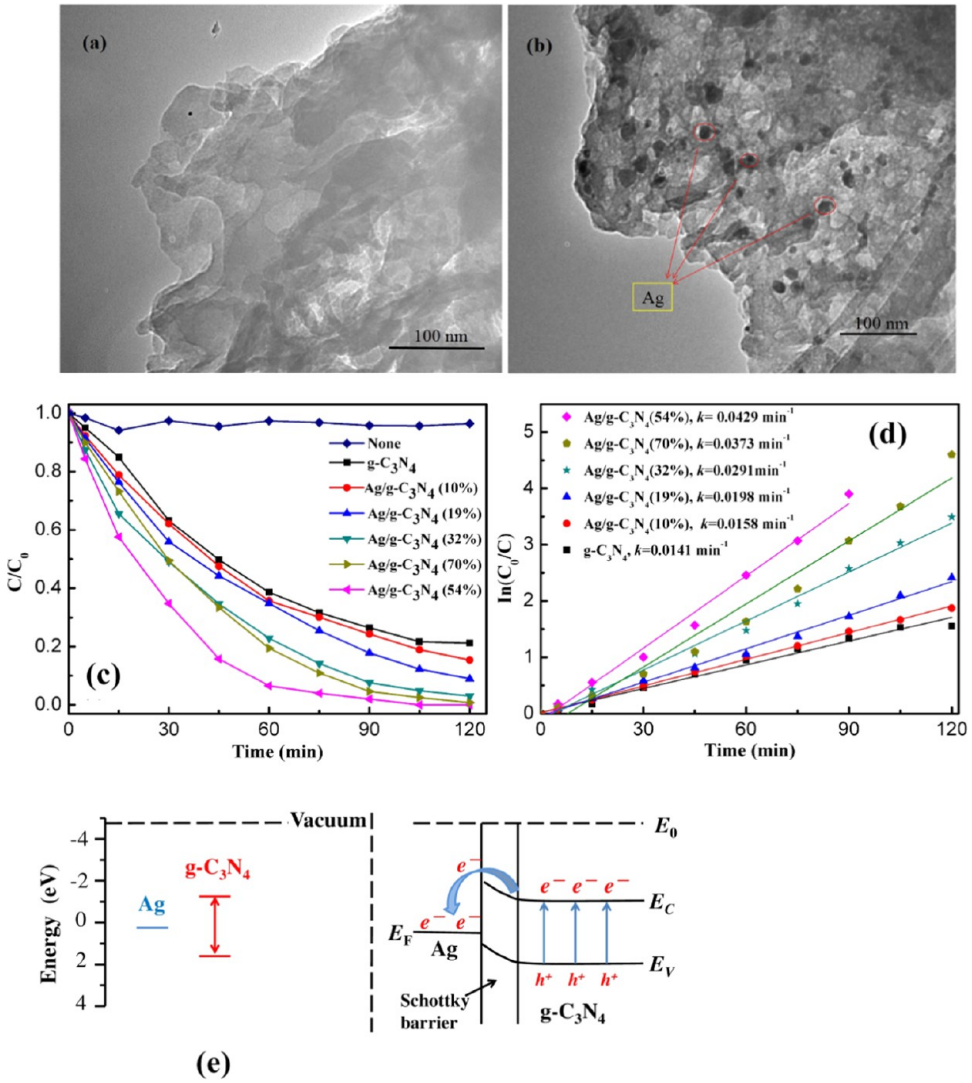

Figure 3. Transmission electron microscopy (TEM) images of (a) pure g-C_3N_4 and (b) Ag/g-C_3N_4(54%) composites. (c) Photodegradation of DCF with different photocatalysts under visible light. (d) Plot of $\ln(C_0/C)$ vs irradiation time for DCF representing the fit using a pseudo-first-order reaction rate. (e) Formation of Schottky barrier for the contact of Ag and g-C_3N_4. Adapted with permission from ref 67. Copyright 2016 Elsevier.

DOI: 10.1021/acsami.8b03620
ACS Appl. Mater. Interfaces 2018, 10, 21035−21055

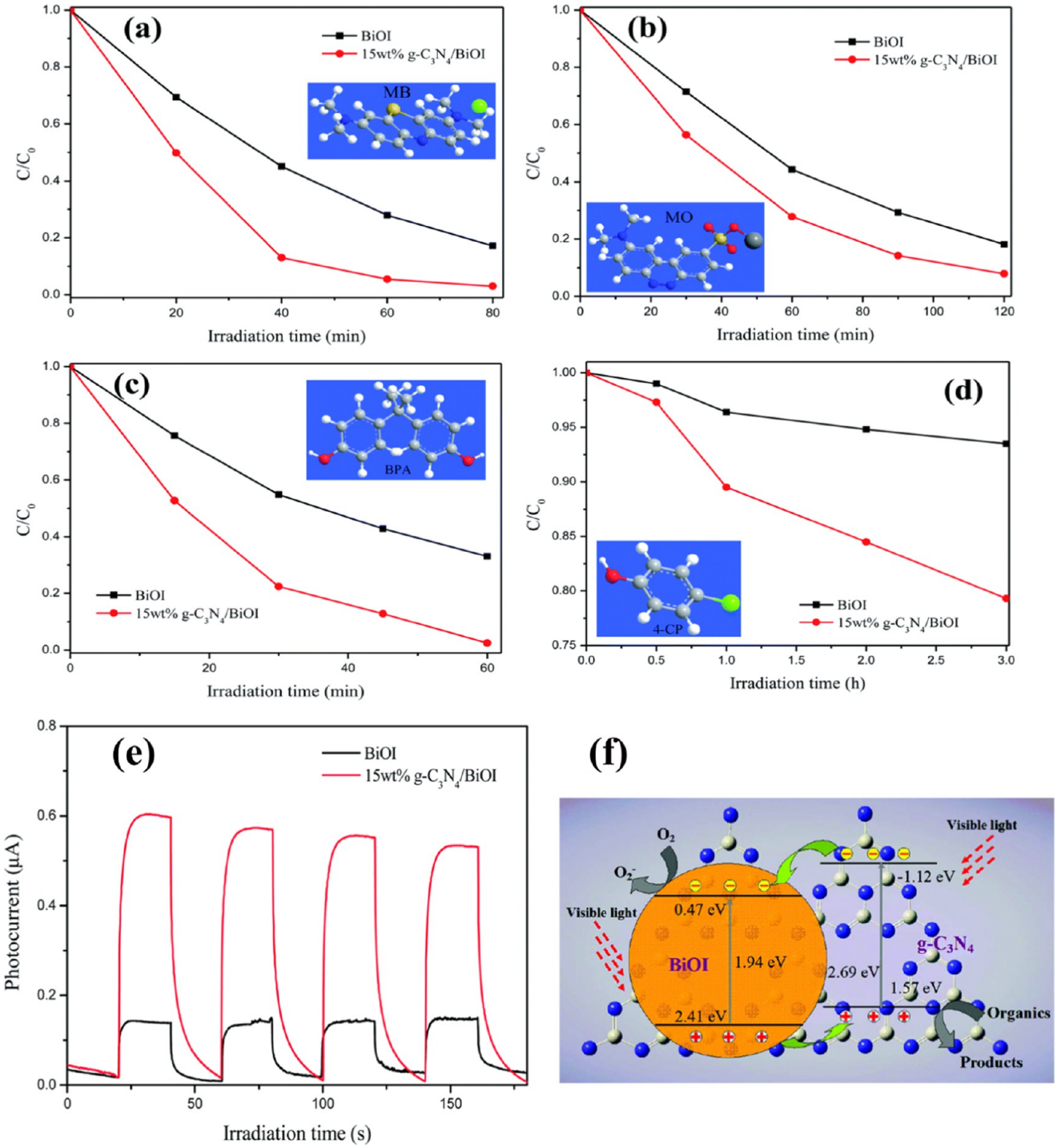

Figure 4. Photocatalytic degradation of (a) MB, (b) MO, (c) BPA, and (d) 4-CP in the presence of BiOI, with 15 wt % g-C_3N_4/BiOI under visible light irradiation. (e) Transient photocurrent response for pure BiOI and 15 wt % g-C_3N_4/BiOI composite. (f) Schematic of the separation and transfer of photogenerated charges in g-C_3N_4/BiOI combined with the possible reaction mechanism of photocatalytic procedure. Adapted with permission from ref 81. Copyright 2014 Royal Society of Chemistry.

on the surface of photocatalysts, accelerating the photocorrosion process of the photocatalysts themselves.[44] Therefore, construction of hierarchical structure of GBH is a workable approach to increase the efficiency of photocatalysis, which can significantly accelerate the surface reaction kinetics.

2.2. Photocatalytic Treatment of Persistent Organic Pollutants by g-C_3N_4-Based Heterojunction Photocatalyst. With the development of industrialization, poisonous and harmful pollutants are continuously discharged into the environment. These pollutants not only cause various environmental problems, but also pose a serious threat to human health.[45] Among the various contaminants, persistent organic pollutants (POPs), such as polycyclic aromatic hydrocarbons, polychlorinated biphenyls, and pentachlorophenol, have led to severe environmental pollution.[46] With persistence, bioaccumulation, mobility, and high toxicity, typical POPs can exist in the environment for a long time and migrate everywhere.[47] Therefore, POPs have become the research hot spot in the field

DOI: 10.1021/acsami.8b03620
ACS Appl. Mater. Interfaces 2018, 10, 21035−21055

of environmental, chemical, and environmental toxicology.[48] Hence, photodegradation of POPs over semiconductor solids has attracted extensive research attention recently. A more comprehensive list of POPS treatment by GBH is summarized in Table 1. The photocatalytic treatment of POPs over GBH reported in the literature could be divided into two types: photocatalytic oxidation and photocatalytic reduction.

2.2.1. Oxidative Degradation of POPs by g-C_3N_4-Based Heterojunction Photocatalyst. Many studies have been carried out to explore the photodegradation of organic dyes in aqueous solution over GBH photocatalyst in the last few years, which show an obvious increase of the photocatalytic ability. For instance, rhodamine B (RhB) can be degraded by g-C_3N_4/Bi_2MoO_6 heterojunctions.[66] Methyl orange (MO) can be degraded by Co_3O_4/g-C_3N_4 heterojunctions.[67,68] In recent years, POPs have gradually become the focus of research, such as the degradation of 4-chlorophenol (4-CP) over the g-C_3N_4/ZnO heterojunction photocatalyst[64] and the degradation of 2,4-dibromophenol by Z-scheme Bi_2MoO_6/CNTs/g-C_3N_4 heterojunction photocatalyst.[69] At the same time, molecular imprinting technology can be applied to the photocatalyst to remove target POPs.[70]

To date, many types of metal/g-C_3N_4 nanocomposite system, such as Ag/g-C_3N_4 and Cu/g-C_3N_4, have been designed.[71,72] In addition, some bimetallic/g-C_3N_4 systems, for example, AuPd/g-C_3N_4 and PtCo/g-C_3N_4 also been designed for improving photocatalytic properties of g-C_3N_4.[73,74] These metal/g-C_3N_4 nanocomposites show intensive photocatalytic activity, in which the Schottky junction plays a decisive role in diminishing the recombination of photoinduced electron−hole pairs. In addition, as an excellent semiconductor, g-C_3N_4 could combine with other metals to form Schottky junctions for treatment of POPs. For example, the Ag/g-C_3N_4 heterostructure is used for the photocatalytic degradation of diclofenac (DCF).

In the study conducted by Zhang et al., Ag/g-C_3N_4 heterostructured photocatalysts were synthesized via photodeposition in ambient condition.[71] Under experimental conditions, the results of DCF degradation by the as-prepared samples showed that the photocatalytic performance of optimum Ag/g-C_3N_4 (54%) was 3.1 times higher than pure g-C_3N_4 (Figure 3d,e). Nevertheless, the photocatalytic activity was limited by excess loading of Ag. This may be due to the fact that at low loading, Ag can act as the sink for electrons to diminish the recombination of photoinduced carriers. But at a high loading, Ag acts as a new center of electron−hole pair recombination and covers g-C_3N_4.[71]

The corresponding scavengers are used to quench the specific reactive species for trapping experiments of radicals (isopropyl alcohol (10 mM) for $^{\bullet}OH$, benzoquinone (0.5 μM) for $^{\bullet}O_2^-$, sodium azide (0.5 μM) for $^1O_2$, and ethylenediaminetetraacetic acid (EDTA) disodium (5 μM) for holes).[75,76] After addition of EDTA disodium, the degradation of DCF was inhibited obviously, which indicated that holes play a major role and other reactive species have no obvious effect in the degradation of DCF in the Ag/g-C_3N_4 photocatalytic system. Because of the Schottky junctions, the electron−hole pairs could be effectively separated in the metal−semiconductor interface. From the thermodynamic viewpoint, the CB of g-C_3N_4 (−1.3 V vs NHE) is more negative than Ag^+/Ag (0.80 V vs NHE). Therefore, the photogenerated electrons on the CB of the g-C_3N_4 can reduce Ag^+ to metallic Ag again in situ and transfer the electron to oxygen via electron-transfer routes.[23,77]

Except for Schottky junction, POPs can undergo photodegradation by other GBH types effectively.[78,79] For example, the efficiency of photodegradation of acid orange-II by g-C_3N_4/$Bi_4Ti_3O_{12}$ heterojunction has been significantly improved due to the formation of heterojunction structure. In addition, the results are also confirmed by the study of Yin et al.[80] In the study conducted by Di et al., the g-C_3N_4/BiOI heterojunction was synthesized via one-pot EG-assisted solvothermal process for photodegradation of 4-CP and bisphenol A (BPA).[81] The photodegradation activity of MB and MO demonstrated that the photodegradation efficiency of g-C_3N_4/BiOI heterojunction was far higher than pure BiOI (Figure 4a,b). The optimal g-C_3N_4/BiOI composite has an enhancement of about 30% for the BPA degradation compared to the pure BiOI (Figure 4c). In addition, the results of photodegradation of 4-CP indicated that the photocatalytic activity of the optimal g-C_3N_4/BiOI composite was much higher than that of pure BiOI (Figure 4d). The photocurrent intensity of the optimal g-C_3N_4/BiOI was nearly 3.5 times higher than that of single BiOI, which indicated that the formation of heterojunction could inhibit recombination of photoinduced carriers and promote transfer of interfacial charge (Figure 4e). The mechanism of g-C_3N_4/BiOI heterojunction is shown in Figure 4f. Because the CB of g-C_3N_4 is more negative than that of BiOI and the VB of BiOI is more positive than that of g-C_3N_4, photogenerated electrons are migrated from the CB of g-C_3N_4 to the CB of BiOI. Synchronously, the holes on the VB of BiOI migrate to those of g-C_3N_4. Thus, the photoinduced electrons and holes could separate effectively and the lifetime of photogenerated carriers could be prolonged.

2.2.2. Photocatalytic Reduction of Persistent Organic Pollutants by g-C_3N_4-Based Heterojunction Photocatalyst. Development of efficient photocatalysts with excellent photoinduced oxidation and reduction properties is of great significance to environment remediation and energy storage. In addition to photooxidation, it is found that photocatalytic reduction, another important function of semiconductor-based photocatalysts, suggests a great promising in the research of environmental remediation. In recent years, photocatalytic reduction has attracted the attention of many researchers. Many compounds have been photocatalytically reduced, such as polybromodiphenyl ethers, perchlorinated compounds, and nitro compounds.[82−86] Because of the electron, donor can scavenge VB holes, thus diminishing the recombination of photoinduced carriers within the particle and freeing more reductive equivalents in these studies. We can find that the photocatalytic reduction efficiency will be increased due to the addition of electron donor in the reaction system.

In the study conducted by Dai et al., the CdS/g-C_3N_4 heterojunction was prepared by a hydrothermal method for nitrobenzene photoreduction.[87] Yang et al. found an accessible method for preparing heterostructured MIL-125/Ag/g-C_3N_4 nanocomposites for the reduction of nitrobenzene under visible light illumination.[88] All of these studies show that the photoreduction efficiency of GBH photocatalyst was better than that of pure g-C_3N_4.

A simple self-assembly photochemical reduction method was developed by Zhang et al. to prepare highly photocatalytic TiO_2 nanowire/g-C_3N_4 nanosheet/graphene heterostructure (TiO_2 NWs/g-C_3N_4/G) for the selective reduction of nitrobenzene.[89] The scanning electron microscopy (SEM) and TEM images show that the three materials are combined well with good morphology (Figure 5a,b). Under experimental conditions, the

DOI: 10.1021/acsami.8b03620
ACS Appl. Mater. Interfaces 2018, 10, 21035−21055

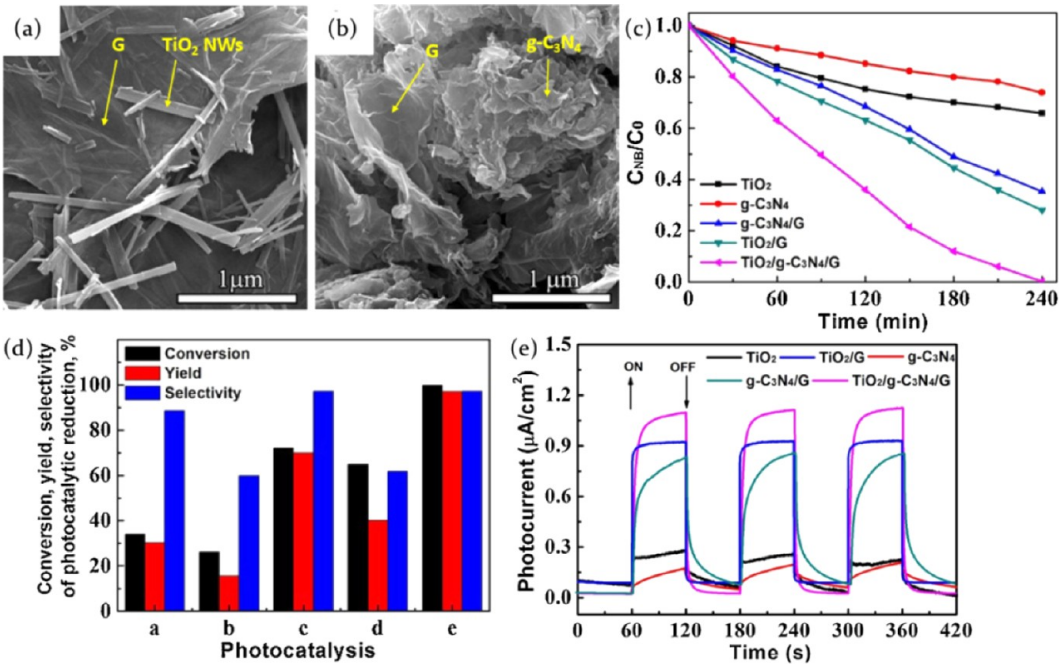

Figure 5. (a) SEM and (b) TEM images of TiO_2/g-C_3N_4/G. (c) Photoreduction curves of the NB aqueous solutions containing different photocatalysts. (d) Conversion, yield, and selectivity of photocatalytic reduction ((a) TiO_2 NWs; (b) g-C_3N_4; (c) TiO_2/G; (d) g-C_3N_4/G; (e) TiO_2/g-C_3N_4/G). (e) Photocurrent response of the photoanodes of TiO_2 NWs, g-C_3N_4, TiO_2/G, g-C_3N_4/G, and TiO_2/g-C_3N_4/G samples. Adapted with permission from ref 90. Copyright 2017 Elsevier.

TiO_2/g-C_3N_4/G composite exhibits the highest photocatalytic reduction efficiency of 97%, which is much higher than that of TiO_2/G, g-C_3N_4/G, pure TiO_2, and g-C_3N_4 (Figure 5c,d). The photoelectrochemical (PEC) performances of TiO_2/g-C_3N_4/G composites showed the highest photocurrent of 1.1 μA cm^2, which means more photogenerated electrons are excited and transferred (Figure 5e). The above results show that the heterojunction formation between TiO_2 nanowire, g-C_3N_4 nanosheet, and graphene led to the improvement of photocatalytic activity.

2.3. Heavy-Metal-Ion Redox by g-C_3N_4-Based Heterojunction Photocatalyst. Due to the fact that they cannot be biodegraded but can accumulate in biological tissues and causes serious danger to organism, heavy-metal ions are more harmful than organic pollutants.[90−93] In the process of industrial production, hexavalent chromium (Cr(VI)) discharged into natural water can cause a serious environmental pollution.[94−97] Cr(VI) is known to be a mutagenic, carcinogenic, and toxic substance, which is harmful to biological systems and human body.[98] At present, many treatment methods have been explored to repair heavy-metal pollution, such as physical methods, chemical methods, biological methods, synergistic combination of nanomaterials and microbes, and so on.[99−101] Notably, photocatalytic reduction is considered as an environment-friendly technology for efficient elimination of Cr(VI) contaminants by utilizing sunlight and attracts more and more attention with the advantages of mild reaction conditions and absence of secondary pollution among many treatment methods.[100,101] Arsenic (As) and its compounds are common pollutants in the environment, which may cause various adverse effects in the human body, such as gastrointestinal, cardiovascular, respiratory, genotoxic, and dermal changes, as well as mutagenic and carcinogenic effects.[102,103] In contrast to Cr, the toxicity of As in the reduced state (As(III)) is higher than that in the oxidized state (As(V)). Therefore, the oxidation of As(III) to As(V) is beneficial for reducing and finally removing toxicity.[104] In sum, the well-designed GBH is a good candidate for heavy-metal pollution remediation.

Charlton et al. used a thermal transformation methodology to fabricate a visible light response heterostructure of g-C_3N_4/TiO_2.[105] After 100 min of visible light irradiation, the Cr(VI) photoreduction efficiencies of pure TiO_2 and optimized composite were 20 and 72%, respectively. The synergistic heterojunction formation between g-C_3N_4 nanosheets with doped TiO_2 was the primary reason for the enhancement of photoreduction of Cr(VI). Xin et al. synthesized a heterojunction of Ag−$Sr_{0.25}H_{1.5}Ta_2O_6{\cdot}H_2O$/g-$C_3N_4$, which showed excellent visible light photocatalytic activity for Cr(VI) reduction and MO degradation.[106] The high-resolution TEM (HRTEM) and TEM images showed that g-C_3N_4 served as the support to bind $Sr_{0.25}H_{1.5}Ta_2O_6{\cdot}H_2O$ nanoparticles in heterojunction system (Figure 6). Under experimental conditions, the rate constant of Cr (VI) photoreduction by the optimized composite (0.57 ± 0.07 h^{-1}) was 2 times and 500 times higher compared to pure g-C_3N_4 and $Sr_{0.25}H_{1.5}Ta_2O_6{\cdot}H_2O$, respectively. Due to the formation of heterojunction and using Ag as an electron mediator, the recombination efficiency of electron−hole pair has been greatly diminished. In addition, the photogenerated electrons can readily move to the CB of $Sr_{0.25}H_{1.5}Ta_2O_6{\cdot}H_2O$ from g-C_3N_4 because the CB of g-C_3N_4 is more negative than that of $Sr_{0.25}H_{1.5}Ta_2O_6{\cdot}H_2O$. Then, the photogenerated electrons could react with $Cr_2O_7^{2-}$ or O_2 leading to the photoreduction of Cr(VI) or formation of $O_2^{\bullet-}$ active species. Moreover, both holes in the VB of g-C_3N_4 and the $O_2^{\bullet-}$ active species could lead to the degradation of methyl orange.

Through a facile one-pot synthesis, α-Fe_2O_3/g-C_3N_4 heterojunction composites were prepared by Sun et al., which showed excellent performance under visible light on synchronous photocatalytic oxidation and adsorption of As(III) in

DOI: 10.1021/acsami.8b03620
ACS Appl. Mater. Interfaces 2018, 10, 21035−21055

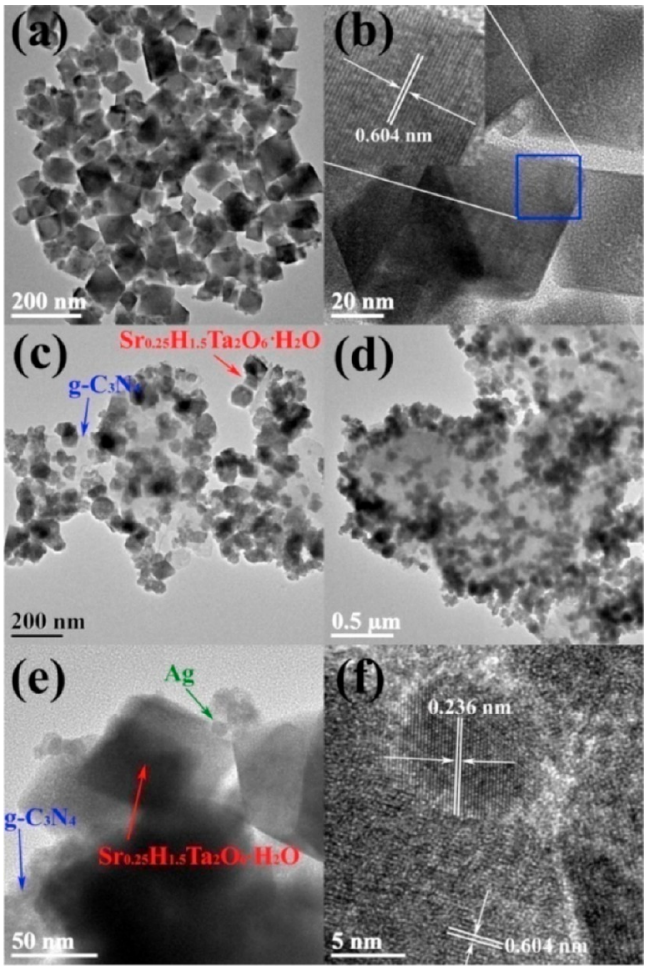

Figure 6. TEM (a) and HRTEM (b) images of pure $Sr_{0.25}H_{1.5}Ta_2O_6 \cdot H_2O$ nanoparticles; TEM images of $Sr_{0.25}H_{1.5}Ta_2O_6 \cdot H_2O$/g-$C_3N_4$ heterojunction (c) and Ag−$Sr_{0.25}H_{1.5}Ta_2O_6 \cdot H_2O$/g-$C_3N_4$ (d). High-magnification TEM (e) and HRTEM (f) images of Ag−$Sr_{0.25}H_{1.5}Ta_2O_6 \cdot H_2O$/g-$C_3N_4$. Adapted with permission from ref 105. Copyright 2016 Elsevier.

aqueous solution.[107] Under both high-resolution transmission electron microscope and transmission electron microscope, 12% Fe-CN presents three lattice fringes: one with d = 0.32 nm matches the (002) crystal interplanar of g-C_3N_4 and the others with d = 0.25 and 0.27 nm match the (110) and (104) planes of α-Fe_2O_3, which indicated that the heterojunction structure successfully formed between g-C_3N_4 and α-Fe_2O_3 (Figure 7a,b).[108] In addition, the photocatalysis rate constant over the optimized sample is 0.0047 min^{-1}, which is about 5.9 and 11.8 times higher than that of pure g-C_3N_4 and α-Fe_2O_3, respectively. According to the above results, the heterojunction structure between g-C_3N_4 and α-Fe_2O_3 is the primary reason for the enhancement of As removal.

2.4. Oxidative Decomposition of Pathogens by GBH Photocatalyst. In recent decades, pathogens in drinking water sources have been prevalently found, creating a serious problem for human health and ecosystem balance.[109,110] Pathogens such as a variety of helminthes, fungi, bacteria, protozoa, rickettsiae, viruses, and prions can cause many kinds of waterborne infectious agents. Therefore, disinfection of water has become an urgent problem in environmental protection. Many methods were applied to control waterborne pathogens in water bodies, including multiple-barrier approaches and effective photon-

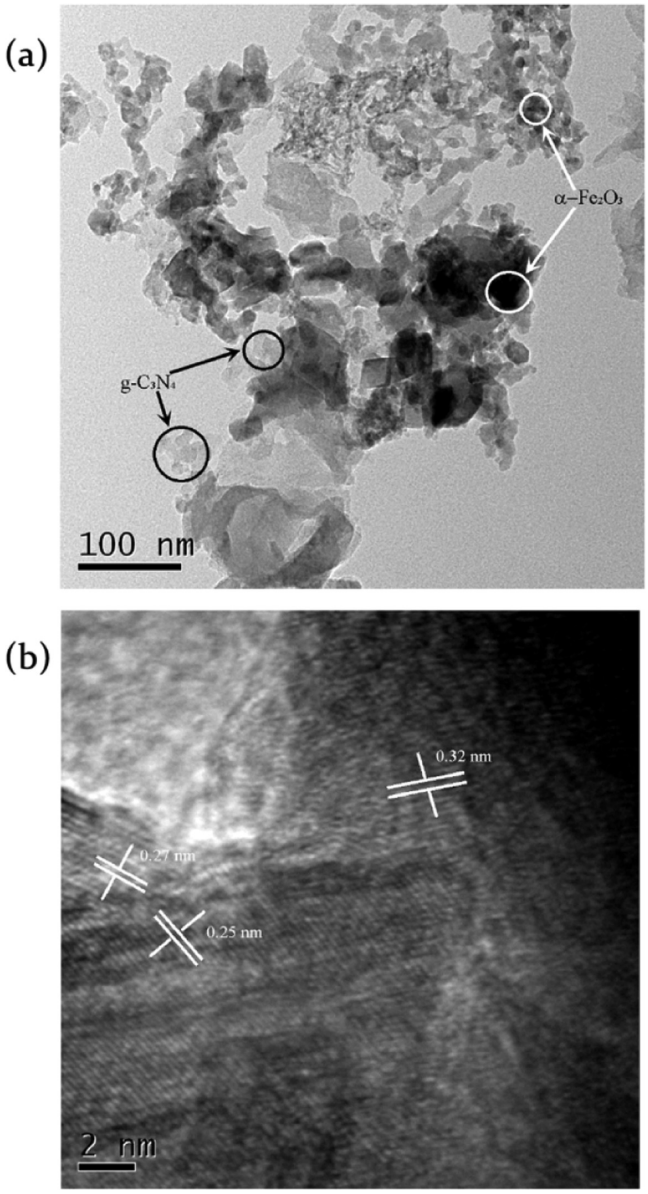

Figure 7. (a) TEM and (b) HRTEM images of 12% Fe-CN. Reprinted with permission from ref 106. Copyright 2017 Elsevier.

based chemical inactivation.[1] Among the many treatments mentioned above, photocatalytic inactivation of pathogens has received increasing attention in recent years as an environmentally friendly and efficient method.[111] Several studies have paid attention to disinfection by GBH because of its excellent visible light response performance and higher electron−hole pair separation efficiency. Xia et al. reported the application of a Z-scheme g-C_3N_4/m-Bi_2O_4 heterojunction for inactivation of *Escherichia coli K-12*.[112] Under illumination of visible light, the 6 log_{10} cfu mL^{-1} of *E. coli K-12* could be completely inactivated within 1.5 h by the optimized g-C_3N_4/m-Bi_2O_4 heterojunction, which was 1.9 times and 5 times higher than pure Bi_2O_4 and g-C_3N_4, respectively.

Wang et al. wrapped reduced graphene oxide (RGO) and g-C_3N_4 (CN) sheets on crystals of cyclooctasulfur (α-S_8) by different orders to form two distinctive structures of metal-free heterojunction photocatalysts.[113] Interestingly, CN/RGO/α-S_8 showed relatively better photocatalytic performance in aerobic conditions and RGO/CN/α-S_8 was more dynamic in anaerobic

DOI: 10.1021/acsami.8b03620
ACS Appl. Mater. Interfaces 2018, 10, 21035−21055

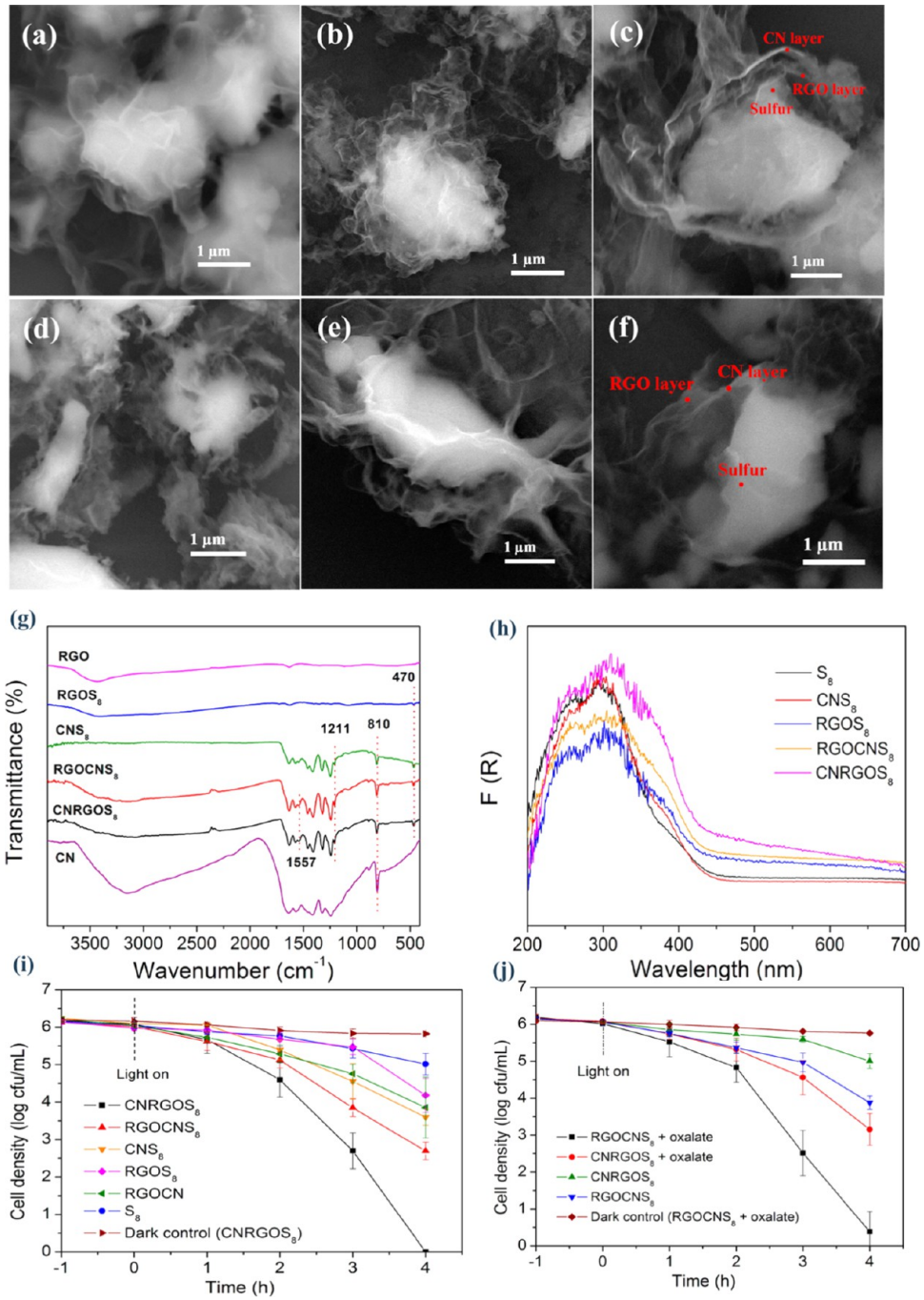

Figure 8. SEM images of (a) RGOS8, (b) CNRGOS8, (c) cross section of CNRGOS8 microspheres, (d) CNS8, (e) RGOCNS8, and (f) cross section of RGOCNS8 microspheres. UV−vis DRS (g) and FTIR (h) spectra of the RGO and CN sheets co-wrapped with α-sulfur. Photocatalytic inactivation efficiency against *E. coli K-12* (2×10^6 cfu mL^{-1}, 50 mL) in the presence of the as-prepared samples in (i) aerobic condition and (j) anaerobic condition under VL irradiation. No inactivation occurs in the dark and light controls. Reprinted with permission from ref 112. Copyright 2013 American Chemical Society.

condition under visible light irradiation. The SEM images clearly show that both samples are two-layered structures (Figure 8). As shown in Figure 8g, the UV−vis diffuse reflectance spectroscopy (DRS) results of the as-prepared sample demonstrated that RGO/CN/α-S_8 and CN/RGO/α-S_8 show a more significant red shift compared to bare α-S_8, CN/α-S_8, and RGO/α-S_8. Because the CN sheets were wrapped at the outer layer of α-S_8, CN/RGO/α-S_8 obtained a more red shift than RGO/CN/α-S_8. Under aerobic condition, the bacterial inactivation efficiency of CN/RGO/α-S_8 was about 1.7 times, 3 times, 3.3 times, and 7 times higher than that of RGO/CN/α-S_8, CN/α-S_8, RGO/α-S_8, and α-S_8, respectively (Figure 8i). The photocatalytic inactivation efficiency of both CN/RGO/α-S_8 and RGO/CN/α-S_8 decreased significantly under the anaerobic condition, which owing to the photoinduced electron−hole pairs would recombine more easily without O_2 (Figure 8j). Interestingly, the CN/RGO/α-S_8 showed a slightly higher inactivation efficiency compared to RGO/CN/α-S_8, probably due to the electrons which play a crucial role in the inactivation of bacterial cells in anaerobic condition. Moreover,

DOI: 10.1021/acsami.8b03620
ACS Appl. Mater. Interfaces 2018, 10, 21035−21055

Table 2. H_2 Yields of Different g-C_3N_4-Based Heterojunctions

photocatalysts	types of heterojunction	H_2 evolution rate (μmol h^{-1} g^{-1})	ref (year)
g-C_3N_4/SiC	type II	182	119 (2017)
Bi_2MoO_6/g-C_3N_4	type II	563.4	120 (2017)
$CoTiO_3$/g-C_3N_4	Z-scheme	858	121 (2016)
g-C_3N_4/WS_2	type II	101	122 (2015)
MoS_2/g-C_3N_4	type II	231	123 (2014)
Ta_2O_5/g-C_3N_4	type II	36.4	118 (2017)
Cu_2O/g-C_3N_4	type II	33.2	124 (2018)
NGQDs-$ZnNb_2O_6$/g-C_3N_4	type II	223.2	125 (2017)
RGO/g-C_3N_4	type II	55.8	126 (2018)
$Cd_{0.5}Zn_{0.5}S$@UIO-66@g-C_3N_4	type II	1281.1	127 (2017)
MoS_2/g-C_3N_4	type II	1420	128 (2018)
g-C_3N_4/Ni/NiS	type II	515	129 (2017)
red phosphor/g-C_3N_4	type II	1000	130 (2013)
g-C_3N_4/OD-ZnO	Z-scheme	322	64 (2017)
CdS/g-C_3N_4	type II	4152	131 (2013)
g-C_3N_4/NiS	type II	447.7	132 (2014)
g-C_3N_4/WO_3	Z-scheme	28.4	133 (2015)
$CaIn_2S_4$/g-C_3N_4	type I	102	134 (2015)
g-C_3N_4/CoO	type II	651.3	135 (2017)

the RGO sheets in the outer layer could inject electron into bacterial cells because of the high mobility of photogenerated electrons on graphene.[114] The increased electron capture by bacterial cells could in turn increase electron−hole pair separation of RGO/CN/α-S_8, which results in the increase of photocatalytic activity.

3. APPLICATIONS OF G-C_3N_4-BASED HETEROJUNCTION IN ENERGY STORAGE

3.1. H_2 Evolution Reaction. As is known to all, solar energy is the most abundant energy in the world as a clean energy. For a long time, preparation of hydrogen (H_2) by semiconductor-based photocatalysts from water splitting is considered a promising method for solar energy storage.[115] H_2 is a promising renewable energy with virtues of no carbon emission, high energy density, and production of a useful byproduct (water) from combustion.[116] However, at present, H_2 is mainly produced by the conversion of fossil fuels by steam reforming, which is seriously restricted due to its low efficiency and high cost.[117] It is well known that nature abundantly stores H_2 in the form of water. Consequently, Wang et al. applied g-C_3N_4 in photocatalytic H_2 evolution from water splitting under visible light irradiation in the presence of a sacrificial donor for the first time in 2009.[12] Nevertheless, the H_2 yield of pure g-C_3N_4 was relatively low and observed to fluctuate and *d* showed discrepancy from one batch to other (0.1−4 μmol h^{-1}).

To tackle this problem, many researchers formed heterojunction between g-C_3N_4 and other nanomaterials to improve efficiency for H_2 evolution. The H_2 yields of different GBHs are summarized in Table 2. Lately, Hong et al. have prepared Ta_2O_5/g-C_3N_4 heterojunctions by a simple one-step heating method.[118] The obtained heterojunctions showed obvious improvement of H_2 production compared to pure g-C_3N_4. Under experimental conditions, the photocatalytic H_2 yield of the optimized Ta_2O_5/g-C_3N_4 heterojunction (36.4 μmol h^{-1} g^{-1}) was about 4.2 times higher than that of pure g-C_3N_4 (8.7 μmol h^{-1} g^{-1}). In addition, H_2 evolution reaction of the optimized Ta_2O_5/g-C_3N_4 heterojunction sample was sustained for over 20 h without obvious deactivation, indicating its excellent photochemical stability. Moreover, electrochemical impedance spectroscopy (EIS) spectra and photoluminescence (PL) emission spectra of the samples show that the enhancement of photocatalytic activity is mainly due to the interfacial charge separation in the heterojunction between g-C_3N_4 and Ta_2O_5 (Figure 9a,b).

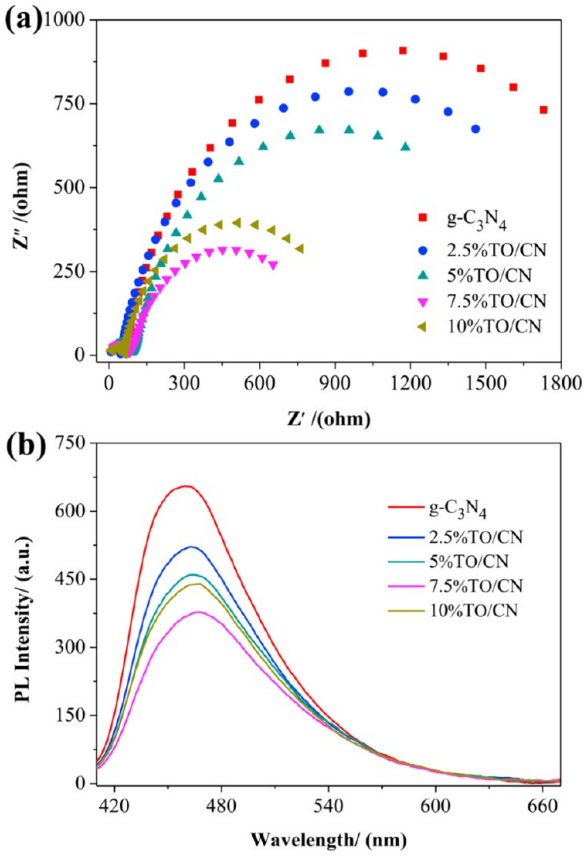

Figure 9. (a) EIS spectra and (b) PL emission spectra of as-prepared samples. Reprinted with permission from ref 118. Copyright 2016 Elsevier.

DOI: 10.1021/acsami.8b03620
ACS Appl. Mater. Interfaces 2018, 10, 21035−21055

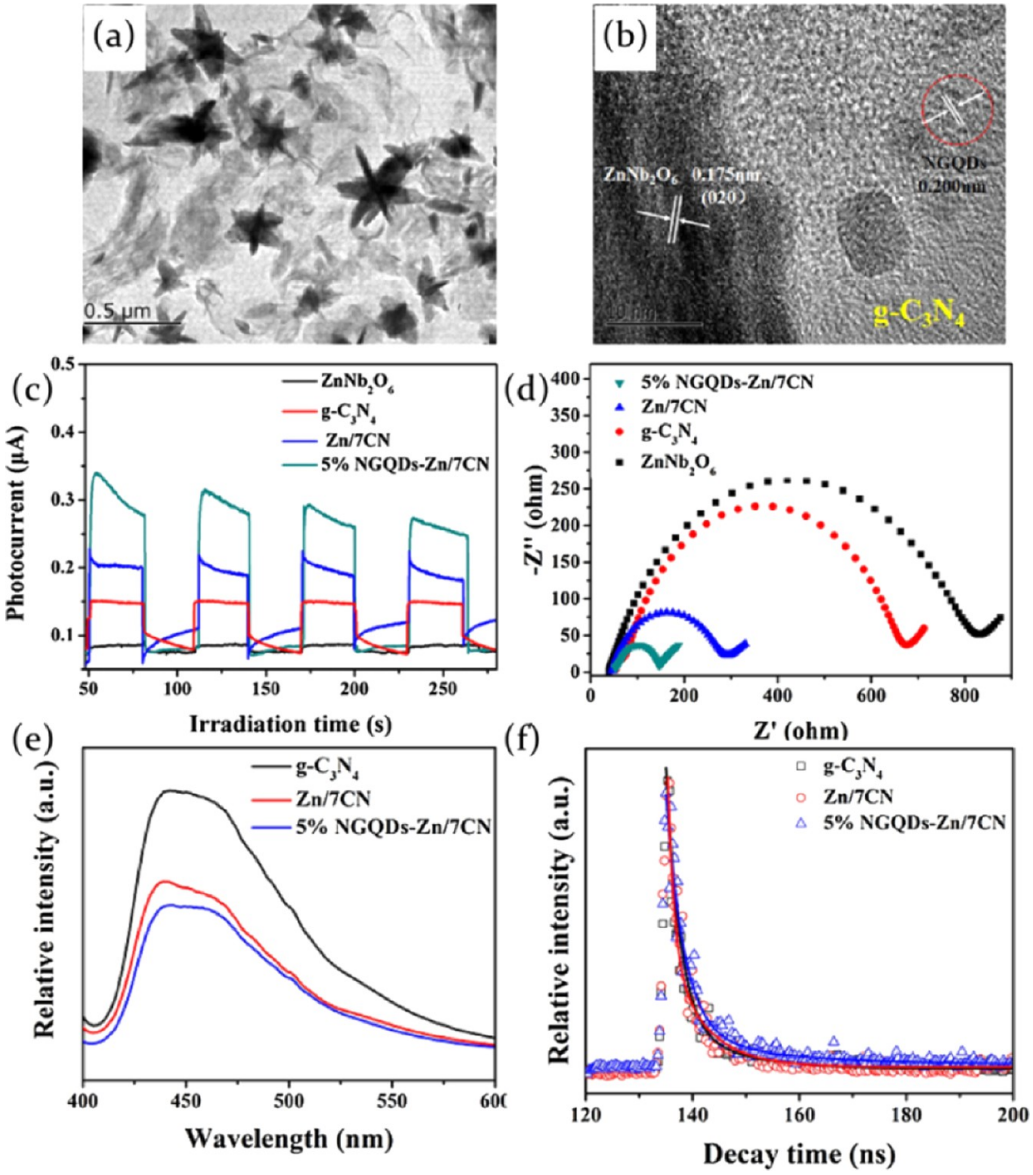

Figure 10. (a) TEM and (b) HRTEM images of 5% NGQDs-Zn/7CN. (c) Transient photocurrent response and (d) EIS spectra for pure $ZnNb_2O_6$, g-C_3N_4, Zn/7CN, and 5% NGQDs-Zn/7CN samples. (e) PL spectra and (f) fluorescence decay curves of g-C_3N_4, Zn/7CN, and 5% NGQDs-Zn/7CN. Reprinted with permission from ref 120. Copyright 2017 Elsevier.

Yan and co-workers investigated a novel photocatalyst that employed nitrogen-doped graphene quantum dots (NGQDs) $ZnNb_2O_6$/g-C_3N_4 (NGQDs-Zn/CN) heterostructures.[125] As shown in Figure 10a,b, the TEM and HRTEM images of 5% NGQDs-Zn/7CN (Zn/CN mole ratio, 1/7; amount of NGQDs, 5%) sample showed that $ZnNb_2O_6$ and g-C_3N_4 were close enough and mixed with each other and NGQDs were attached to the surface of g-C_3N_4. H_2 production activity of the as-prepared samples was carried out in 20% methyl alcohol solution with 1% Pt as a co-catalyst. Under experimental conditions, the 5% NGQDs-Zn/7CN heterojunctions showed the highest photocatalytic efficiency (340.9 μmol h^{-1} g^{-1}), which was about 3.2 times and 1.5 times higher compared to pure g-C_3N_4 (103.7 μmol h^{-1} g^{-1}) and Zn/CN (223.2 μmol h^{-1} g^{-1}). In addition, repeated experiments of 5% NGQDs-Zn/7CN heterojunctions indicated that it has good stability during the photocatalytic reaction. In Figure 10c, the photocurrent with all of the samples showed that the 5% NGQDs-Zn/7CN has the highest photocurrent response, which indicated that the formation of heterojunction was conducive to interfacial charge transfer and photoinduced electron−hole pair separation. The EIS spectra of all of the samples in Figure 10d also show that the 5% NGQDs-Zn/7CN sample exhibited the best smallest arc radius. It is well known that the smaller radius of the Nyquist circle means faster interfacial charge transfer and more effective separation of electrons and holes. In addition, the 5% NGQDs-Zn/7CN showed the lowest PL emission intensity and the longest calculated average lifetime of 5.23 ns (Figure 10e,f). These results demonstrated that the recombination of photoinduced carriers was suppressed and more charge carriers participated in photocatalytic water splitting in the 5% NGQDs-Zn/7CN heterojunction system.

3.2. CO_2 Reduction by g-C_3N_4-Based Heterojunction Photocatalyst. The carbon cycle plays a key role in the stability of global ecological balance.[136] But along with the fast

DOI: 10.1021/acsami.8b03620
ACS Appl. Mater. Interfaces 2018, 10, 21035−21055

Table 3. Hydrocarbon Yield of CO_2 Reduction by Different g-C_3N_4-Based Heterojunctions

photocatalysts	type of heterojunctions	hydrocarbon yields	ref (year)
MnO_2/g-C_3N_4	Z-scheme	68 μmol h^{-1} g^{-1} (CO)	138 (2017)
g-C_3N_4/SnS_2	Z-scheme	2.3 μmol h^{-1} g^{-1} (CH_3OH), 0.64 μmol h^{-1} g^{-1} (CH_4)	143 (2017)
g-C_3N_4/NiAl-LDH	type II	8.2 μmol h^{-1} g^{-1} (CO)	144 (2018)
red phosphor/g-C_3N_4	type II	295 μmol h^{-1} g^{-1} (CH_4)	130 (2013)
α-Fe_2O_3/g-C_3N_4	Z-scheme	27.2 μmol h^{-1} g^{-1} (CO)	145 (2018)
g-C_3N_4/N-TiO_2	type II	12.2 μmol h^{-1} g^{-1} (CO)	146 (2014)
g-C_3N_4/Bi_2WO_6	Z-scheme	5.19 μmol h^{-1} g^{-1} (CO)	147 (2015)
BiOI/g-C_3N_4	Z-scheme	3.44 μmol h^{-1} g^{-1} (CO), 0.16 μmol h^{-1} g^{-1} (CH_4), 0.37 μmol h^{-1} g^{-1} (H_2), 1.89 μmol h^{-1} g^{-1} (O_2)	148 (2016)
g-C_3N_4/$Bi_4O_5I_2$	Z-scheme	45.6 μmol h^{-1} g^{-1} (CO), 6 μmol h^{-1} g^{-1} (CH_4), 10 μmol h^{-1} g^{-1} (H_2), 2 μmol h^{-1} g^{-1} (O_2)	142 (2016)
SnO_2/g-C_3N_4	Z-scheme	18 μmol h^{-1} g^{-1} (CO), 3 μmol h^{-1} g^{-1} (CH_3OH), 2 μmol h^{-1} g^{-1} (CH_4)	149 (2015)
WO_3/g-C_3N_4	Z-scheme	19.4 μmol h^{-1} g^{-1} (CH_3OH)	150 (2014)
ZnO/g-C_3N_4	Z-scheme	0.6 μmol h^{-1} g^{-1} (CH_3OH)	151 (2015)
Co_4/g-C_3N_4	type II	89.6 μmol h^{-1} g^{-1} (CO), 5.8 μmol h^{-1} g^{-1} (H_2)	152 (2017)

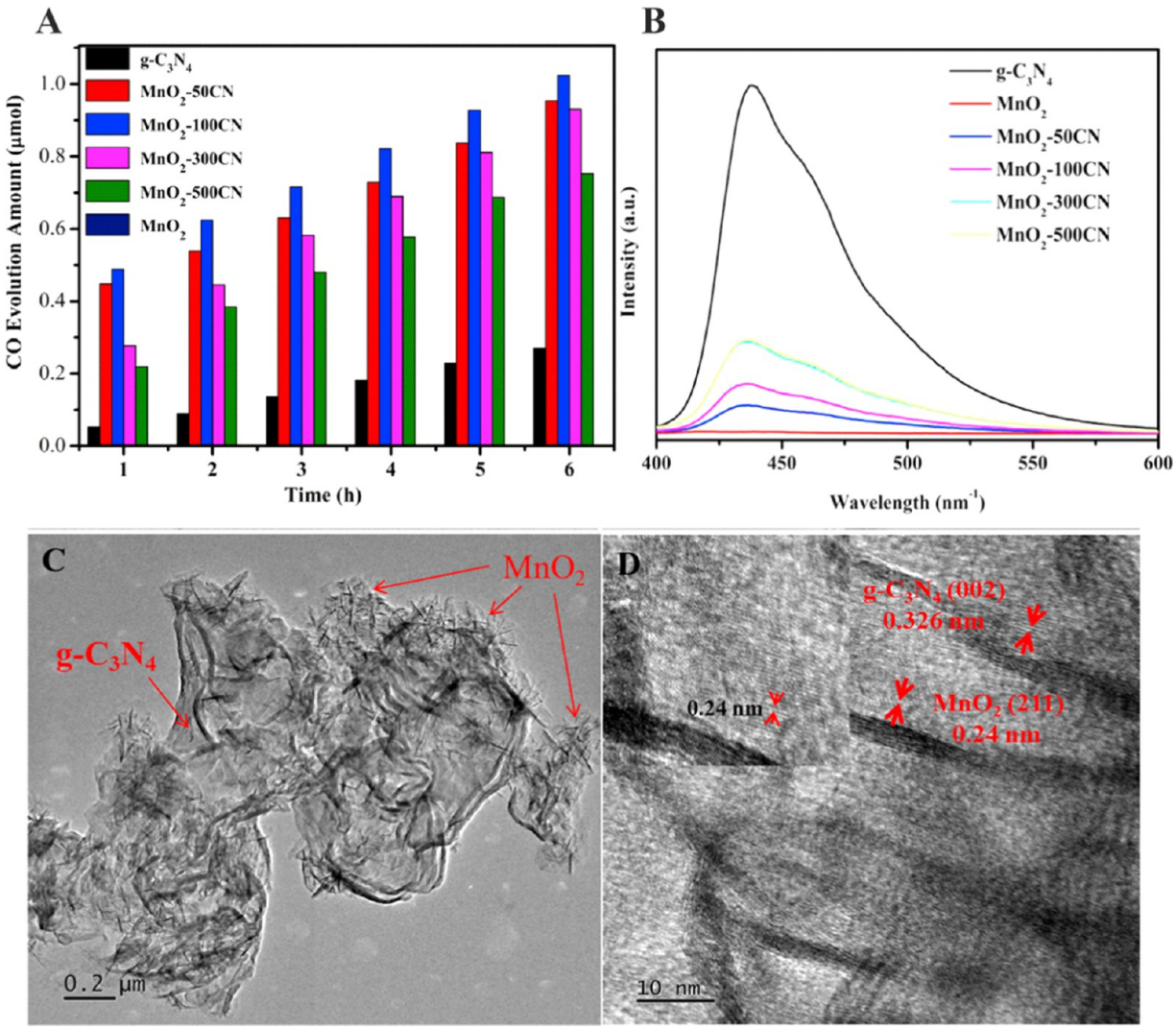

Figure 11. (A) Time-dependent CO generation over synthesized g-C_3N_4, MnO_2, and MnO_2/g-C_3N_4 catalysts. (B) PL spectra (excitation wavelength: 380 nm) of g-C_3N_4, MnO_2, and MnO_2/g-C_3N_4 samples. (C) TEM and (D) HRTEM images of MnO_2-100CN. Reprinted with permission from ref 138. Copyright 2017 Elsevier.

development of industry, the extensive use of fossil fuels emits more CO_2, which not only affects the carbon cycle and leads to greenhouse effect, but also creates an energy crisis.[137] In recent years, the rapid development of the photocatalytic technology has become one of the best ways to solve these problems through converting CO_2 into chemical fuels, for instance, CO, methane, and methanol, which has aroused much research attention.[138−140] Because of the good stability of CO_2, the photoreduction of CO_2 over photocatalyst under ambient pressure, room temperature, and visible light irradiation

DOI: 10.1021/acsami.8b03620
ACS Appl. Mater. Interfaces 2018, 10, 21035−21055

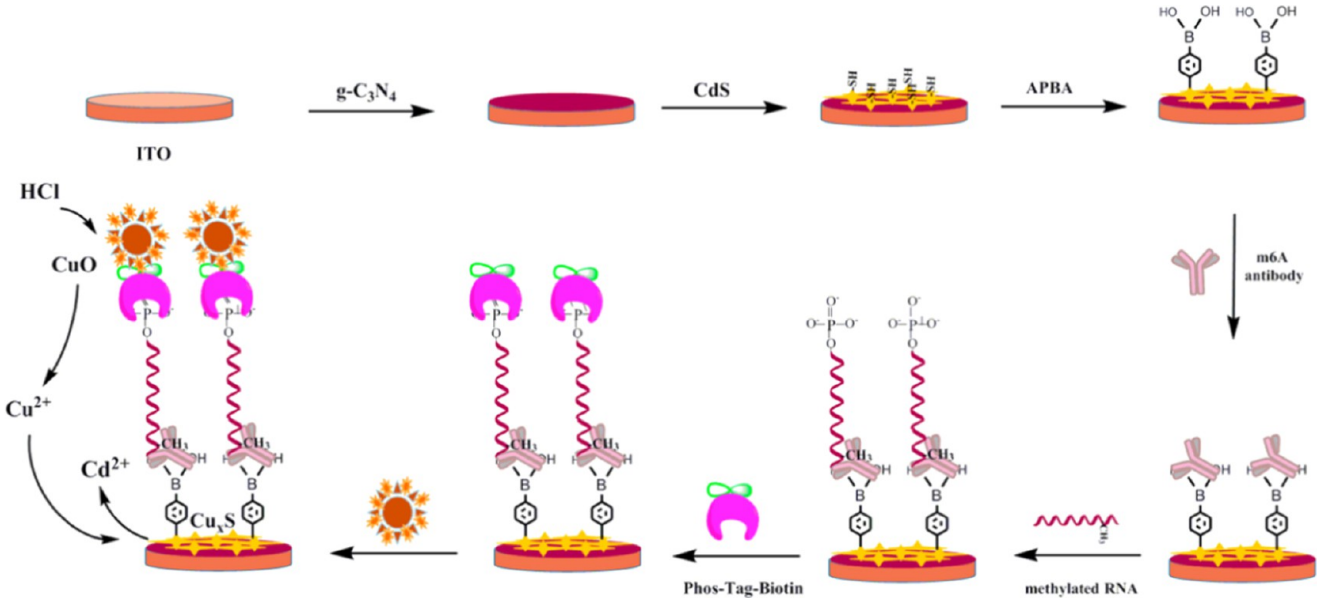

Figure 12. Schematic representation of the PEC biosensor construction process and detection strategy. Reprinted with permission from ref 158. Copyright 2017 Elsevier.

continues to present a great challenge, which results in the need of a better photocatalyst to solve this problem.[141] The hydrocarbon yield of CO_2 reduction by different GBHs is summarized in Table 3. Bai and co-workers prepared a novel Z-scheme g-C_3N_4/$Bi_4O_5I_2$ heterojunction for increase photoreduction activity of CO_2.[142] Di et al. synthesized a Z-scheme g-C_3N_4/SnS_2 heterojunction by a simple one-step hydrothermal method.[143] According to X-ray photoelectron spectroscopy and DFT calculations, the interfacial IEF formed when the electrons move from g-C_3N_4 to SnS_2. Therefore, the IEF-induced direct Z-scheme charge-transfer mechanism occurred in the g-C_3N_4/SnS_2 heterojunction system, which illustrates the enhanced photocatalytic activity as well as the improved CO_2 reduction efficiency.

Recently, a hierarchical Z-scheme α-Fe_2O_3/g-C_3N_4 photocatalyst for reduction of CO_2 to CO has been synthesized by Jiang and co-workers.[145] Under experimental conditions, the CO evolution rate of the optimized composite (27.2 μmol h^{-1} g^{-1}) without co-catalyst and sacrifice reagent was 2.2 times higher than that of pure g-C_3N_4 (10.3 μmol h^{-1} g^{-1}). Furthermore, only 7% attenuation was observed after four consecutive runs with each run of 4 h under irradiation. The separation of photoinduced electron−hole pairs was facilitated, and the reduction ability of the photoinduced electrons was promoted after the formation of Z-scheme heterojunction between α-Fe_2O_3 and g-C_3N_4.

Wang et al. synthesized a novel MnO_2/g-C_3N_4 heterojunction by an in situ redox reaction between potassium permanganate ($KMnO_4$) and manganese sulfate ($MnSO_4$) adsorbed on the surface of g-C_3N_4, which exhibited good performance in the photoreduction of CO_2.[138] Under TEM and HRTEM, the MnO_2/g-C_3N_4 composites showed that two components are in intimate linkage with each other (Figure 11C,D). The N_2 adsorption/desorption measurements showed that the specific surface area of MnO_2/g-C_3N_4 heterojunction composites was higher compared to pure g-C_3N_4 and MnO_2, which is beneficial to expose active sites and improve the CO_2 adsorption capacity. According to PL analysis of all samples, pure g-C_3N_4 exhibited the highest intensity and MnO_2/g-C_3N_4 composites showed obvious decrease after improving the load of MnO_2, which indicated that the formation of heterojunction was beneficial for the separation of photoinduced carriers (Figure 11B). Under experimental conditions, the amount of CO produced from optimal MnO_2/g-C_3N_4 was 20.4 μmol g^{-1} after 6 h, which was 4 times higher than that from pure g-C_3N_4 (3.4 μmol g^{-1}) (Figure 11A). And the optimal sample showed a high structure stability after recycling photocatalytic tests. Under illumination condition, the holes on the VB of MnO_2 are caught by H_2O molecule to generate protons and O_2. Moreover, the electrons on the CB of g-C_3N_4 react with CO_2 adsorbed on the surface of photocatalyst to produce CO and H_2O with the participation of photons.

4. OTHER EMERGING APPLICATIONS OF G-C_3N_4-BASED HETEROJUNCTION

4.1. Biosensor. In the last few years, photoelectrochemcial (PEC) sensors have received much attention for their low background current, low cost, fast response, and high detection sensitivity. In numerous studies, GBH nanomaterials show great potential as a photoactive material with excellent PEC biosensing property due to their high visible light absorption efficiency and separation rate of photoinduced carriers. Liu and co-workers developed a label-free photoelectrochemical (PEC) aptasensor for adenosine detection based on CdS/polypyrrole/g-C_3N_4 nanocomposites.[153] The CdS/g-C_3N_4 heterojunction could improve photo-to-current conversion efficiency by preventing photogenerated charge recombination of g-C_3N_4 and self-photocorrosion processes of CdS effectively. Moreover, the minimum adenosine detection was 0.1 nmol L^{-1}, which indicated that the aptasensor shows better adenosine detection performance than many reported methods, for example, chemiluminescence, fluorescence, and electrochemistry.[154−156]

PEC sensors in which GBH acts as a photosensitive material can also be used for the detection of some difficult-to-detect substances. Several studies have shown a close association between the level of dynamic N^6-methyladenosine (m^6A) and certain diseases, especially cancer, which indicated the importance of dynamic m^6A level in biology.[157] Although the

DOI: 10.1021/acsami.8b03620
ACS Appl. Mater. Interfaces 2018, 10, 21035−21055

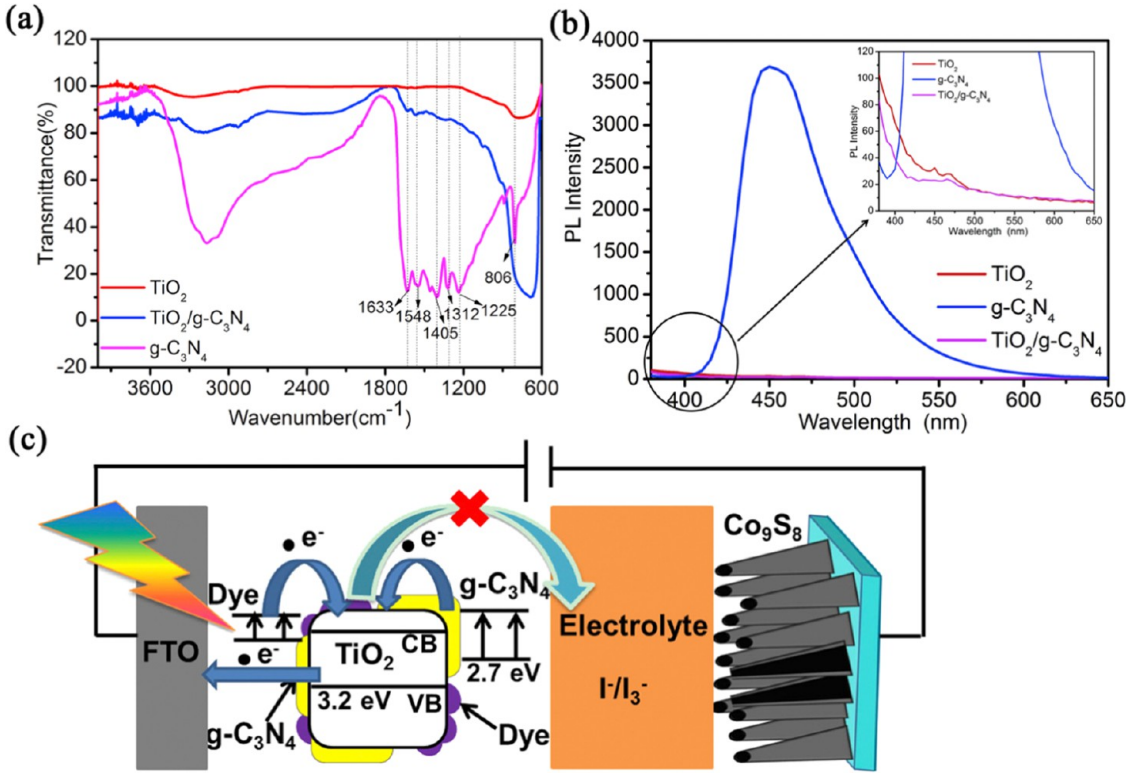

Figure 13. (a) FTIR spectra of TiO_2, g-C_3N_4, and TiO_2/g-C_3N_4 powder. (b) PL spectra of TiO_2, g-C_3N_4, and TiO_2/g-C_3N_4 (inset is the enlarged image of the circled part of the PL spectra). (c) Schematic diagram of g-C_3N_4 as blocking layer and Co_9S_8 as counter electrode to increase the power conversion efficiency of DSSCs. Reprinted with permission from ref 164. Copyright 2017 Elsevier.

importance of m^6A has been proved, the quantitative detection of m^6A has been greatly restricted due to the reactionlessness of the methyl group, low content of mRNA, and interference of potential RNA structures around the methylation site. Consequently, it is important to develop an effective and rapid method for m^6A detection. Under the circumstances, Wang et al. used g-C_3N_4/CdS quantum dots (g-C_3N_4/CdS) heterojunction to construct a novel PEC immunosensor for m^6A detection based on the inhibition of Cu^{2+} to the photoactivity of g-C_3N_4/CdS heterojunction.[158] The PEC biosensor construction process and detection strategy are shown in Figure 12. Electrodes are treated by different methods, and the photocurrent response was recorded to verify the detection feasibility of the PEC assay. The photocurrent response became much stronger than individual g-C_3N_4/ITO and CdS/ITO when CdS QDs are attached on the g-C_3N_4/ITO electrode. This indicated that CdS QDs as photosensitive material can be greatly promoted by the photocurrent response of g-C_3N_4. In addition, further studies show that absence of methylated RNA could lead to the absence of Cu^{2+}, which could assemble Phos-tag-biotin and avidin-CuO on CdS/g-C_3N_4/ITO electrode surface. Under optimal conditions, the lowest detection limit of novel PEC immunosensor was 3.53 pM, which presented a wide linear range (0.01−10 nM) and good detection selectivity of m^6A-methylated RNA.

4.2. Solar Cells. With the continuous development of society, the demand for energy has been increasing. In recent years, the overuse of fossil fuel has resulted in the depletion of oil reserves present on the earth.[159] Environmental contamination and greenhouse effect caused by the combustion of fossil dyes have also become a major problem that human beings need to face. These problems drive scientists to find a clean, renewable energy instead of fossil fuels. Because of its abundance and continuous energy supply, solar energy has attracted wide attention of researchers.[160] In recent years, many solar devices have been developed, including solar cells due to their decisive advantages of lightweight, flexibility, and low module cost over conventional silicon-based solar modules.[161]

As a key part of solar cells, photoanodes can harvest light efficiently and improve the utilization efficiency of solar energy. As a narrow band gap semiconductor, g-C_3N_4 has strong visible light-absorbing ability to improve the solar cell performance. Xu and co-workers used g-C_3N_4/TiO_2 composites to fabricate dye-sensitized solar cells (DSSCs), which showed approximately 28% enhancement of power conversion efficiency at optimal loading amount of g-C_3N_4.[162] Ansari et al. used g-C_3N_4 nanotube/ZnO nanorod composites as photoanode materials and CdS quantum dots as sensitizing materials to fabricate quantum dots-sensitized solar cell, which shows 32% energy conversion efficiency compared to the g-C_3N_4 nanoflakes-based device.[163] It is indicated that the photovoltaic properties of photoanode materials could be improved by changing the physical properties of the materials. And composite materials showed superior performance to single materials. As an excellent semiconductor nanomaterial, GBHs are also used for the fabrication of solar cells, particularly DSSCs because of their unique features.

In the study conducted by Yuan and co-workers, high-performance DSSCs were reported based on rationally designed g-C_3N_4-modified TiO_2 nanosheets as photoanodes and Co_9S_8 nanotube arrays as counter electrodes (CEs).[164] Because of the strong interaction between TiO_2 and g-C_3N_4, the FTIR spectra of samples showed that the Ti−O−Ti

DOI: 10.1021/acsami.8b03620
ACS Appl. Mater. Interfaces 2018, 10, 21035−21055

stretching vibration of TiO_2/g-C_3N_4 spectrum exhibits a large red shift compared to pure TiO_2 (Figure 13a). The results of PL spectroscopy analyses in Figure 13b show that the PL emission intensity of TiO_2/g-C_3N_4 nanocomposites significantly decreases compared to pure g-C_3N_4, indicating that the separation rate of photoinduced carriers increased due to the formation of heterojunction. The photovoltaic parameters of DSSCs based on the different photoanodes and counter electrodes (CEs) showed that DSSCs based on TiO_2/g-C_3N_4 electrodes exhibit the best conversion efficiency (8.07%), which is attributed to the g-C_3N_4 layer acting as a barrier layer to restrain the recombination of charge at the TiO_2/electrolyte interface. The conversion efficiency of DSSCs based on TiO_2/g-C_3N_4 electrodes is 1.3 times higher than that of DSSCs based on TiO_2 photoanodes (6.19%). Moreover, the open-circuit potential (V_{oc}), short-circuit current density (J_{sc}), and conversion efficiency (η) all increased compared to those of the DSSCs based on TiO_2 photoanode after loading g-C_3N_4 layer on TiO_2 nanosheet surface.

The mechanism of improving the performance of solar cells is shown in Figure 13c. Because the CB position of TiO_2 is more positive than g-C_3N_4, electrons in the CB of TiO_2 cannot move to g-C_3N_4. Therefore, the electron concentration in the photoanodes has been increased, which could enhance the performance of DSSC. In addition, due to the strong interaction and heterostructure between TiO_2 and g-C_3N_4, the performance of DSSCs improved remarkably.

All of the studies covered in this review showed that multifunction applications of GBH photoactive nanocomposites will help us move into a truly sustainable era.

5. CONCLUSIONS AND PROSPECT

In the past several years, many studies have proven that a good design of GBH nanocomposite can overcome many problems of single-phase semiconductor among the various photoactive applications. Therefore, it is the right time to provide a comprehensive and state-of-the-art review on the applications and mechanism of GBH. In this review, the photocatalytic mechanisms of GBH on the basis of first-principles calculations and thermodynamics and kinetics of surface catalytic reaction are discussed. In addition, a concise appraisal of the latest research results of GBHs is presented, such as photocatalytic treatment of persistent organic pollutants, heavy-metal-ion redox, oxidative decomposition of pathogens, water splitting for H_2 evolution, CO_2 reduction, solar cells, and biosensors. All of these applications exhibited good performances. However, although researchers have made progress in these areas, practical large-scale application and commercialization of GBH photoactive nanocomposites are still subject to many limitations.

First, it is still a great challenge to develop a facile, efficient, and economic method for preparing materials to achieve mass production of materials for practical applications. Second, due to the importance of the interface properties of the heterojunction nanocomposite, the rational design of the heterojunction nanocomposites is indispensable by an excellent preparation method. Third, light corrosion and/or photodegradation of photoactive nanocomposite have received considerable attention for the most of photoreaction system. Photoactive nanomaterials with good performance but short lifetime are not good choices for large-scale applications. Last but not least, agglomeration of nanomaterials is a serious problem in the process of practical application because of various reasons. Under laboratory conditions, we often use magnetic stirring to solve this problem. However, this problem needs a better solution in large-scale practical applications.

For these reasons, further substantial progress is required in engineering highly efficient, low cost, and environmentally friendly GBH photoactive nanomaterials. We concluded that several aspects will benefit future research: (1) The synthesis of heterojunction photoactive nanomaterials with specific morphology is a direction worth studying, which will further enhance the various aspects of the nanomaterial properties. (2) Use the theoretical calculations and modeling methods to predict the performance and charge-transport process of heterojunction nanocomposites, which facilitate our more targeted design of specific applications of heterojunction nanocomposites and predict whether the material can solve our problem successfully. Not only these methods can save research resources, but also deeper understanding of the mechanisms can be achieved to help us design heterojunction nanocomposites more reasonably. (3) Most of the existing works focus on how to improve the efficiency of GBH photoactive nanocomposite, but the influence of nanomaterials on environment and biology is often neglected. Therefore, we believe that researchers should pay more attention to the environmental effect of photoactive nanomaterials so as to avoid the secondary pollution of large-scale applications of GBH photoactive nanomaterials in subsequent studies. Meanwhile, the recycling and reuse of materials also need to be concerned, in particular the interaction between GBH photoactive nanomaterials and reactive oxygen species. Although some studies have shown that g-C_3N_4 has excellent stability in the presence of organic pollutants under illumination and slightly decomposes when attacked by abundant hydroxyl radical directly, further research is required to explore the photocorrosion of the GBH.[165] In conclusion, the research on GBH photoactive nanocomposite is at its infancy and more interesting properties need to be explored. We hope this review will give researchers a little incentive to develop more suitable heterojunction photoactive nanomaterials that can be applied in a large scale to achieve environmental protection and produce clean energy. In conclusion, we believe that true sustainability can be achieved in the near future by the joint efforts of all scientists.

■ AUTHOR INFORMATION

Corresponding Authors

*E-mail: huangdanlian@hnu.edu.cn. Tel: +86-731-88823701 (D.H.).

*E-mail: ym8188@hnu.edu.cn. Tel: +86-153-88908900 (M.Y.).

ORCID

Danlian Huang: 0000-0003-4955-5755

Guangming Zeng: 0000-0002-4230-7647

Notes

The authors declare no competing financial interest.

■ ACKNOWLEDGMENTS

This study was supported by the Program for the National Natural Science Foundation of China (51579098, 51779090, 51709101, 51278176, 51408206, and 51521006), the National Program for Support of Top−notch Young Professionals of China (2014), Hunan Provincial Science and Technology Plan Project (No. 2016RS3026), and the Program for Changjiang

DOI: 10.1021/acsami.8b03620
ACS Appl. Mater. Interfaces 2018, 10, 21035−21055

Scholars and Innovative Research Team in University (IRT-13R17).

REFERENCES

(1) Shannon, M. A.; Bohn, P. W.; Elimelech, M.; Georgiadis, J. G.; Mariñas, B. J.; Mayes, A. M. Science and Technology for Water Purification in the Coming Decades. *Nature* **2008**, *452*, 301−310.

(2) Chen, F.; Yang, Q.; Wang, S.; Yao, F.; Sun, J.; Wang, Y.; Zhang, C.; Li, X.; Niu, C.; Wang, D.; Zeng, G. Graphene Oxide and Carbon Nitride Nanosheets Co-modified Silver Chromate Nanoparticles with Enhanced Visible-light Photoactivity and Anti-photocorrosion Properties towards Multiple Refractory Pollutants Degradation. *Appl. Catal., B* **2017**, *209*, 493−505.

(3) Fujishima, A.; Honda, K. Photolysis-Decomposition of Water at the Surface of an Irradiated Semiconductor. *Nature* **1972**, *238*, 37−38.

(4) Carey, J. H.; Lawrence, J.; Tosine, H. M. Photodechlorination of PCB's in the Presence of Titanium Dioxide in Aqueous Suspensions. *Bull. Environ. Contam. Toxicol.* **1976**, *16*, 697−701.

(5) Tian, J.; Zhao, Z.; Kumar, A.; Boughton, R. I.; Liu, H. Recent Progress in Design, Synthesis, and Applications of One-dimensional TiO_2 Nanostructured Surface Heterostructures: A Review. *Chem. Soc. Rev.* **2014**, *43*, 6920−6937.

(6) Kumar, S. G.; Devi, L. G. Review on Modified TiO_2 Photocatalysis Under UV/Visible Light: Selected Results and Related Mechanisms on Interfacial Charge Carrier Transfer Dynamics. *J. Phys. Chem. A* **2011**, *115*, 13211−13241.

(7) Liu, J.; Liu, Y.; Liu, N.; Han, Y.; Zhang, X.; Huang, H.; Lifshitz, Y.; Lee, S. T.; Zhong, J.; Kang, Z. Water Splitting. Metal-Free Efficient Photocatalyst for Stable Visible Water Splitting via a Two-Electron Pathway. *Science* **2015**, *347*, 970−974.

(8) Huang, D. L.; Wang, R. Z.; Liu, Y. G.; Zeng, G. M.; Lai, C.; Xu, P.; Lu, B. A.; Xu, J. J.; Wang, C.; Huang, C. Application of Molecularly Imprinted Polymers in Wastewater Treatment: A Review. *Environ. Sci. Pollut. Res.* **2015**, *22*, 963−977.

(9) Masih, D.; Ma, Y.; Rohani, S. Graphitic C_3N_4 Based Noble-Metal-Free Photocatalyst Systems: A Review. *Appl. Catal., B* **2017**, *206*, 556−588.

(10) Thomas, A.; Fischer, A.; Goettmann, F.; Antonietti, M.; Müller, J.-O.; Schlögl, R.; Carlsson, J. M. Graphitic Carbon Nitride Materials: Variation of Structure and Morphology and Their Use as Metal-Free Catalysts. *J. Mater. Chem.* **2008**, *18*, 4893−4908.

(11) Redemann, C. E.; Lucas, H. J. Some Derivatives of Cyameluric Acid and Probable Structures of Melam, Melem and Melon. *J. Am. Chem. Soc.* **1940**, *62*, 842−846.

(12) Wang, X.; Maeda, K.; Thomas, A.; Takanabe, K.; Xin, G.; Carlsson, J. M.; Domen, K.; Antonietti, M. A Metal-Free Polymeric Photocatalyst For Hydrogen Production From Water Under Visible Light. *Nat. Mater.* **2009**, *8*, 76−80.

(13) Cui, L.; Ding, X.; Wang, Y.; Shi, H.; Huang, L.; Zuo, Y.; Kang, S. Facile Preparation of Z-scheme WO_3/g-C_3N_4 Composite Photocatalyst with Enhanced Photocatalytic Performance Under Visible Light. *Appl. Surf. Sci.* **2017**, *391*, 202−210.

(14) Zheng, Q.; Durkin, D. P.; Elenewski, J. E.; Sun, Y.; Banek, N. A.; Hua, L.; Chen, H.; Wagner, M. J.; Zhang, W.; Shuai, D. Visible-Light-Responsive Graphitic Carbon Nitride: Rational Design and Photocatalytic Applications for Water Treatment. *Environ. Sci. Technol.* **2016**, *50*, 12938−12948.

(15) Wang, H.; Yuan, X.; Wang, H.; Chen, X.; Wu, Z.; Jiang, L.; Xiong, W.; Zeng, G. Facile Synthesis of Sb_2S_3/ultrathin g-C_3N_4 Sheets Heterostructures Embedded with g-C_3N_4 Quantum Dots with Enhanced NIR-Light Photocatalytic Performance. *Appl. Catal., B* **2016**, *193*, 36−46.

(16) Groenewolt, M.; Antonietti, M. Synthesis of g-C_3N_4 Nanoparticles in Mesoporous Silica Host Matrices †. *Adv. Mater.* **2005**, *17*, 1789−1792.

(17) Wang, K.; Li, Q.; Liu, B.; Cheng, B.; Ho, W.; Yu, J. Sulfur-Doped g-C_3N_4 with Enhanced Photocatalytic CO_2-Reduction Performance. *Appl. Catal., B* **2015**, *176−177*, 44−52.

(18) Cui, Y.; Zhang, G.; Lin, Z.; Wang, X. Condensed and Low-defected Graphitic Carbon Nitride with Enhanced Photocatalytic Hydrogen Evolution under Visible Light Irradiation. *Appl. Catal., B* **2016**, *181*, 413−419.

(19) Wang, X.; Blechert, S.; Antonietti, M. Polymeric Graphitic Carbon Nitride for Heterogeneous Photocatalysis. *ACS Catal.* **2012**, *2*, 1596−1606.

(20) Martin, D. J.; Reardon, P. J. T.; Moniz, S. J.; Tang, J. Visible Light-Driven Pure Water Splitting by a Nature-Inspired Organic Semiconductor-Based System. *J. Am. Chem. Soc.* **2014**, *136*, 12568−12571.

(21) Ye, C.; Li, J.-X.; Li, Z.-J.; Li, X.-B.; Fan, X.-B.; Zhang, L.-P.; Chen, B.; Tung, C.-H.; Wu, L.-Z. Enhanced Driving Force and Charge Separation Efficiency of Protonated g-C_3N_4 For Photocatalytic O_2 Evolution. *ACS Catal.* **2015**, *5*, 6973−6979.

(22) Zhang, S.; Li, J.; Wang, X.; Huang, Y.; Zeng, M.; Xu, J. Rationally Designed 1D Ag@$AgVO_3$ Nanowire/Graphene/Protonated g-C_3N_4 Nanosheet Heterojunctions for Enhanced Photocatalysis via Electrostatic Self-Assembly and Photochemical Reduction Methods. *J. Mater. Chem. A* **2015**, *3*, 10119−10126.

(23) Wang, X.; Maeda, K.; Chen, X.; Takanabe, K.; Domen, K.; Hou, Y.; Fu, X.; Antonietti, M. Polymer Semiconductors for Artificial Photosynthesis: Hydrogen Evolution by Mesoporous Graphitic Carbon Nitride with Visible Light. *J. Am. Chem. Soc.* **2009**, *131*, 1680−1681.

(24) Wu, X.; Liu, C.; Li, X.; Zhang, X.; Wang, C.; Liu, Y. Effect of Morphology on the Photocatalytic Activity of g-C_3N_4 Photocatalysts Under Visible-Light Irradiation. *Mater. Sci. Semicond. Process.* **2015**, *32*, 76−81.

(25) Zhou, C.; Lai, C.; Huang, D.; Zeng, G.; Zhang, C.; Cheng, M.; Hu, L.; Wan, J.; Xiong, W.; Wen, M.; et al. Highly Porous Carbon Nitride by Supramolecular Preassembly of Monomers for Photocatalytic Removal of Sulfamethazine Under Visible Light Driven. *Appl. Catal., B* **2018**, *220*, 202−210.

(26) Azevedo, S.; de Paiva, R. Structural Stability and Electronic Properties of Carbon-Boron Nitride Compounds. *Europhys. Lett.* **2006**, *75*, 126−132.

(27) Yan, S. C.; Li, Z. S.; Zou, Z. G. Photodegradation of Rhodamine B and Methyl Orange over Boron-Doped g-C_3N_4 Under Visible Light Irradiation. *Langmuir* **2010**, *26*, 3894−3901.

(28) Zhang, X.; Wang, Y.; Liu, B.; Sang, Y.; Liu, H. Heterostructures Construction on TiO_2 Nanobelts: A Powerful Tool for Building High-Performance Photocatalysts. *Appl. Catal., B* **2017**, *202*, 620−641.

(29) Ong, W. J.; Tan, L. L.; Ng, Y. H.; Yong, S. T.; Chai, S. P. Graphitic Carbon Nitride (g-C_3N_4)-Based Photocatalysts for Artificial Photosynthesis and Environmental Remediation: Are We a Step Closer To Achieving Sustainability? *Chem. Rev.* **2016**, *116*, 7159−7359.

(30) Mamba, G.; Mishra, A. K. Graphitic Carbon Nitride (g-C_3N_4) Nanocomposites: A New and Exciting Generation of Visible Light Driven Photocatalysts for Environmental Pollution Remediation. *Appl. Catal., B* **2016**, *198*, 347−377.

(31) Schultz, D. M.; Yoon, T. P. Solar Synthesis: Prospects in Visible Light Photocatalysis. *Science* **2014**, No. 1239176.

(32) Zhu, B.; Xia, P.; Li, Y.; Ho, W.; Yu, J. Fabrication and Photocatalytic Activity Enhanced Mechanism of Direct Z-scheme g-C_3N_4/Ag_2WO_4 Photocatalyst. *Appl. Surf. Sci.* **2017**, *391*, 175−183.

(33) Huang, Z. F.; Song, J.; Wang, X.; Pan, L.; Li, K.; Zhang, X.; Wang, L.; Zou, J. J. Switching Charge Transfer of C_3N_4/$W_{18}O_{49}$ from Type-II to Z-Scheme by Interfacial Band Bending for Highly Efficient Photocatalytic Hydrogen Evolution. *Nano Energy* **2017**, *40*, 308−316.

(34) Low, J.; Yu, J.; Jaroniec, M.; Wageh, S.; Al-Ghamdi, A. A. Heterojunction Photocatalysts. *Adv. Mater.* **2017**, No. 1601694.

(35) Gong, Y.; Li, M.; Li, H.; Wang, Y. ChemInform Abstract: Graphitic Carbon Nitride Polymers: Promising Catalysts or Catalyst Supports for Heterogeneous Oxidation and Hydrogenation. *Green Chem.* **2015**, *17*, 715−736.

(36) Tung, R. T. Recent Advances in Schottky barrier Concepts. *Mater. Sci. Eng., R* **2001**, *35*, 1−138.

DOI: 10.1021/acsami.8b03620
ACS Appl. Mater. Interfaces 2018, 10, 21035−21055

(37) Liang, D.; Jing, T.; Ma, Y.; Hao, J.; Sun, G.; Deng, M. Photocatalytic Properties of g-C_6N_6/g-C_3N_4 Heterostructure: A Theoretical Study. *J. Phys. Chem. C* **2016**, *120*, 24023−24029.
(38) Liu, J. Origin of High Photocatalytic Efficiency in Monolayer g-C_3N_4/CdS Heterostructure: A Hybrid DFT Study. *J. Phys. Chem. C* **2015**, *119*, 28417−28423.
(39) Zhang, X.; Meng, Z.; Rao, D.; Wang, Y.; Shi, Q.; Liu, Y.; Wu, H.; Deng, K.; Liu, H.; Lu, R. Efficient Band Structure Tuning, Charge Separation, and Visible-Light Response in ZrS_2-Based Van der Waals Heterostructures. *Energy Environ. Sci.* **2016**, *9*, 841−849.
(40) Gao, G.; Jiao, Y.; Ma, F.; Jiao, Y.; Waclawik, E.; Du, A. Carbon Nanodot Decorated Graphitic Carbon Nitride: New Insights into the Enhanced Photocatalytic Water Splitting from ab Initio Studies. *Phys. Chem. Chem. Phys.* **2015**, *17*, 31140−31144.
(41) Ran, J.; Zhang, J.; Yu, J.; Jaroniec, M.; Qiao, S. Z. ChemInform Abstract: Earth-Abundant Cocatalysts for Semiconductor-Based Photocatalytic Water Splitting. *Chem. Soc. Rev.* **2014**, *43*, 7787−7812.
(42) Li, J.; Liu, E.; Ma, Y.; Hu, X.; Wan, J.; Sun, L.; Fan, J. Synthesis of MoS_2/g-C_3N_4 nanosheets as 2D heterojunction photocatalysts with enhanced visible light activity. *Appl. Surf. Sci.* **2016**, *364*, 694−702.
(43) Huang, D.; Wang, X.; Zhang, C.; Zeng, G.; Peng, Z.; Zhou, J.; Cheng, M.; Wang, R.; Hu, Z.; Qin, X. Sorptive Removal of Ionizable Antibiotic Sulfamethazine from Aqueous Solution by Graphene Oxide-coated Biochar Nanocomposites: Influencing Factors and Mechanism. *Chemosphere* **2017**, *186*, 414−421.
(44) Li, X.; Yu, J.; Jaroniec, M. Hierarchical Photocatalysts. *Chem. Soc. Rev.* **2016**, *45*, 2603−2636.
(45) Huang, D.; Wang, Y.; Zhang, C.; Zeng, G.; Lai, C.; Wan, J.; Qin, L.; Zeng, Y. Influence of Morphological and Chemical Features of Biochar on Hydrogen Peroxide Activation: Implications on Sulfamethazine Degradation. *RSC Adv.* **2016**, *6*, 73186−73196.
(46) Cheng, M.; Zeng, G.; Huang, D.; Lai, C.; Xu, P.; Zhang, C.; Liu, Y.; Wan, J.; Gong, X.; Zhu, Y. Degradation of Atrazine by a Novel Fenton-like Process and Assessment the Influence on the Treated Soil. *J. Hazard Mater.* **2016**, *312*, 184−191.
(47) Cheng, M.; Zeng, G.; Huang, D.; Yang, C.; Lai, C.; Zhang, C.; Liu, Y. Advantages and Challenges of Tween 80 Surfactant-Enhanced Technologies for the Remediation of Soils Contaminated with Hydrophobic Organic Compounds. *Chem. Eng. J.* **2017**, *314*, 98−113.
(48) Hu, C.; Huang, D.; Zeng, G.; Cheng, M.; Gong, X.; Wang, R.; Xue, W.; Hu, Z.; Liu, Y. The Combination of Fenton Process and Phanerochaete Chrysosporium for the Removal of Bisphenol A in River Sediments: Mechanism Related to Extracellular Enzyme, Organic Acid and Iron. *Chem. Eng. J.* **2018**, *338*, 432−439.
(49) Li, Y.; Wang, J.; Yang, Y.; Yan, Z.; Di, H.; An, Q.; Cao, G. Seed-Induced Growing Various TiO_2 Nanostructures on g-C_3N_4 Nanosheets with Much Enhanced Photocatalytic Activity Under Visible Light. *J. Hazard Mater.* **2015**, *292*, 79−89.
(50) Zhao, W.; Wei, Z.; He, H.; Xu, J.; Li, J.; Yang, S.; Sun, C. Supporting 1-D $AgVO_3$ Nanoribbons on Single Layer 2-D Graphitic Carbon Nitride Ultrathin Nanosheets and Their Excellent Photocatalytic Activities. *Appl. Catal., A* **2015**, *501*, 74−82.
(51) Xu, H.; Yan, J.; Xu, Y.; Song, Y.; Li, H.; Xia, J.; Huang, C.; Wan, H. Novel Visible-Light-Driven AgX/graphite-like C_3N_4 (X = Br, I) Hybrid Materials with Synergistic Photocatalytic Activity. *Appl. Catal., B* **2013**, *129*, 182−193.
(52) Zhang, W.; Sun, Y.; Dong, F.; Zhang, W.; Duan, S.; Zhang, Q. Facile Synthesis of Organic-Inorganic Layered Nanojunctions of g-C_3N_4/$(BiO)_2CO_3$ as Efficient Visible Light Photocatalyst. *Dalton Trans.* **2014**, *43*, 12026−12036.
(53) Zhang, S.; Yang, Y.; Guo, Y.; Guo, W.; Wang, M.; Guo, Y.; Huo, M. Preparation and Enhanced Visible-Light Photocatalytic Activity of Graphitic Carbon Nitride/Bismuth Niobate Heterojunctions. *J. Hazard Mater.* **2013**, *261*, 235−245.
(54) Chen, D.; Wang, K.; Hong, W.; Zong, R.; Yao, W.; Zhu, Y. Visible Light Photoactivity Enhancement via CuTCPP Hybridized g-C_3N_4 Nanocomposite. *Appl. Catal., B* **2015**, *166−167*, 366−373.
(55) Zhang, Z.; Huang, J.; Zhang, M.; Yuan, Q.; Dong, B. Ultrathin Hexagonal SnS_2 Nanosheets Coupled with g-C_3N_4 Nanosheets as 2D/2D Heterojunction Photocatalysts toward High Photocatalytic Activity. *Appl. Catal., B* **2015**, *163*, 298−305.
(56) Yang, L.; Huang, J.; Shi, L.; Cao, L.; Liu, H.; Liu, Y.; Li, Y.; Song, H.; Jie, Y.; Ye, J. Sb Doped SnO_2-Decorated Porous g-C_3N_4 Nanosheet Heterostructures with Enhanced Photocatalytic Activities Under Visible Light Irradiation. *Appl. Catal., B* **2018**, *221*, 670−680.
(57) Hong, Y.; Jiang, Y.; Li, C.; Fan, W.; Xu, Y.; Yan, M.; Shi, W. In-Situ Synthesis of Direct Solid-State Z-scheme V_2O_5/g-C_3N_4 Heterojunctions with Enhanced Visible Light Efficiency in Photocatalytic Degradation of Pollutants. *Appl. Catal., B* **2016**, *180*, 663−673.
(58) Cheng, H. J.; Hou, J.; Takeda, O.; Guo, X. M.; Zhu, H. Unique Z-Scheme 2D/2D Nanosheet Heterojunction Design to Harness Charge Transfer for Photocatalysis. *J. Mater. Chem. A* **2015**, *3*, 11006−11013.
(59) Zhang, F.; Wang, L.; Xiao, M.; Liu, F.; Xu, X.; Du, E. Construction of Direct Solid-State Z-scheme g-C_3N_4/BiOI with Improved Photocatalytic Activity for Microcystin-LR Degradation. *J. Mater. Res.* **2017**, 201−212.
(60) Wu, H.; Li, C.; Che, H.; Hu, H.; Hu, W.; Liu, C.; Ai, J.; Dong, H. Decoration of Mesoporous Co_3O_4 Nanospheres Assembled by Monocrystal Nanodots on g-C_3N_4 to Construct Z-scheme System for Improving Photocatalytic Performance. *Appl. Surf. Sci.* **2018**, *440*, 308−319.
(61) Jiang, D.; Ma, W.; Xiao, P.; Shao, L.; Li, D.; Chen, M. Enhanced Photocatalytic Activity of Graphitic Carbon Nitride/Carbon Nanotube/Bi_2WO_6 Ternary Z-scheme Heterojunction with Carbon Nanotube as Efficient Electron Mediator. *J. Colloid Interface Sci.* **2018**, *512*, 693−700.
(62) Xia, P.; Zhu, B.; Cheng, B.; Yu, J.; Xu, J. 2D/2D g-C_3N_4/MnO_2 Nanocomposite as a Direct Z-scheme Photocatalyst for Enhanced Photocatalytic Activity. *ACS Sustainable Chem. Eng.* **2018**, *6*, 965−973.
(63) Sun, M.; Wang, Y.; Shao, Y.; He, Y.; Zeng, Q.; Liang, H.; Yan, T.; Du, B. Fabrication of a Novel Z-scheme g-C_3N_4/Bi_4O_7 Heterojunction Photocatalyst with Enhanced Visible Light-Driven Activity toward Organic Pollutants. *J. Colloid Interface Sci.* **2017**, *501*, 123−132.
(64) Wang, J.; Xia, Y.; Zhao, H.; Wang, G.; Xiang, L.; Xu, J.; Komarneni, S. Oxygen Defects-Mediated Z-scheme Charge Separation in g-C_3N_4/ZnO Photocatalysts for Enhanced Visible-Light Degradation of 4-Chlorophenol and Hydrogen Evolution. *Appl. Catal., B* **2017**, *206*, 406−416.
(65) Zhou, L.; Zhang, W.; Chen, L.; Deng, H. Z-scheme Mechanism of Photogenerated Carriers for Hybrid Photocatalyst Ag_3PO_4/g-C_3N_4 in Degradation of Sulfamethoxazole. *J. Colloid Interface Sci.* **2017**, *487*, 410−417.
(66) Li, H.; Liu, J.; Hou, W.; Du, N.; Zhang, R.; Tao, X. Synthesis and Characterization of g-C_3N_4/Bi_2MoO_6 Heterojunctions with Enhanced Visible Light Photocatalytic Activity. *Appl. Catal., B* **2014**, *160−161*, 89−97.
(67) Han, C.; Lei, G.; Chen, C.; Li, Y.; Xiao, X.; Zhang, Y.; Guo, L. Novel Visible Light Induced Co_3O_4-g-C_3N_4 Heterojunction Photocatalysts for Efficient Degradation of Methyl Orange. *Appl. Catal., B* **2014**, *147*, 546−553.
(68) Huang, D.; Hu, C.; Zeng, G.; Cheng, M.; Xu, P.; Gong, X.; Wang, R.; Xue, W. Combination of Fenton Processes and Biotreatment for Wastewater Treatment and Soil Remediation. *Sci. Total Environ.* **2017**, *574*, 1599−1610.
(69) Ma, D.; Wu, J.; Gao, M.; Xin, Y.; Chai, C. Enhanced Debromination and Degradation of 2,4-Dibromophenol by an Z-scheme Bi_2MoO_6/CNTs/g-C_3N_4 Visible Light Photocatalyst. *Chem. Eng. J.* **2017**, *316*, 461−470.
(70) Lai, C.; Wang, M.-M.; Zeng, G.-M.; Liu, Y.-G.; Huang, D.-L.; Zhang, C.; Wang, R.-Z.; Xu, P.; Cheng, M.; Huang, C.; et al. Synthesis of surface molecular imprinted TiO_2/graphene photocatalyst and its highly efficient photocatalytic degradation of target pollutant under visible light irradiation. *Appl. Surf. Sci.* **2016**, *390*, 368−376.

DOI: 10.1021/acsami.8b03620
ACS Appl. Mater. Interfaces 2018, 10, 21035−21055

(71) Zhang, W.; Zhou, L.; Deng, H. Ag Modified g-C_3N_4 Composites with Enhanced Visible-Light Photocatalytic Activity for Diclofenac Degradation. *J. Mol. Catal. A: Chem.* **2016**, *423*, 270−276.
(72) Fan, M.; Song, C.; Chen, T.; Yan, X.; Xu, D.; Gu, W.; Shi, W.; Xiao, L. Visible-Light-Drived High Photocatalytic Activities of Cu/g-C_3N_4 Photocatalysts for Hydrogen Production. *RSC Adv.* **2016**, *6*, 34633−34640.
(73) Han, C.; Wu, L.; Ge, L.; Li, Y.; Zhao, Z. AuPd Bimetallic Nanoparticles Decorated Graphitic Carbon Nitride for Highly Efficient Reduction of Water to H_2 Under Visible Light Irradiation. *Carbon* **2015**, *92*, 31−40.
(74) Han, C.; Lu, Y.; Zhang, J.; Ge, L.; Li, Y.; Chen, C.; Xin, Y.; Wu, L.; Fang, S. Novel PtCo Alloy Nanoparticle Decorated 2D g-C_3N_4 Nanosheets with Enhanced Photocatalytic Activity for H_2 Evolution Under Visible Light Irradiation. *J. Mater. Chem. A* **2015**, *3*, 23274−23282.
(75) Palominos, R.; Freer, J.; Mondaca, M. A.; Mansilla, H. D. Evidence for Hole Participation During the Photocatalytic Oxidation of the Antibiotic Flumequine. *J. Photochem. Photobiol., A* **2008**, *193*, 139−145.
(76) Cheng, M.; Zeng, G.; Huang, D.; Cui, L.; Xu, P.; Zhang, C.; Liu, Y. Hydroxyl Radicals Based Advanced Oxidation Processes (AOPs) for Remediation of Soils Contaminated with Organic Compounds: A Review. *Chem. Eng. J.* **2016**, *284*, 582−598.
(77) Huang, H.; He, Y.; Du, X.; Chu, P. K.; Zhang, Y. A General and Facile Approach to Heterostructured Core/Shell $BiVO_4$/BiOI P-N Junction: Room-Temperature In Situ Assembly and Highly Boosted Visible-Light Photocatalysis. *ACS Sustainable Chem. Eng.* **2015**, *3*, 3262−3273.
(78) Guo, Y.; Li, J.; Gao, Z.; Zhu, X.; Liu, Y.; Wei, Z.; Zhao, W.; Sun, C. A Simple and Effective Method for Fabricating Novel P−N Heterojunction Photocatalyst g-C_3N_4/$Bi_4Ti_3O_{12}$ and Its Photocatalytic Performances. *Appl. Catal., B* **2016**, *192*, 57−71.
(79) Dong, G.; Zhang, Y.; Pan, Q.; Qiu, J. A Fantastic Graphitic Carbon Nitride (g-C_3N_4) Material: Electronic Structure, Photocatalytic and Photoelectronic Properties ☆. *J. Photochem. Photobiol., C* **2014**, *20*, 33−50.
(80) Yin, S.; Di, J.; Li, M.; Sun, Y.; Xia, J.; Xu, H.; Fan, W.; Li, H. Ionic Liquid-Assisted Synthesis and Improved Photocatalytic Activity of P-N Junction g-C_3N_4/BiOCl. *J. Mater. Sci.* **2016**, *51*, 4769−4777.
(81) Di, J.; Xia, J.; Yin, S.; Xu, H.; Xu, L.; Xu, Y.; He, M.; Li, H. Preparation of Sphere-Like g-C_3N_4/BiOI Photocatalysts via a Reactable Ionic Liquid for Visible-Light-Driven Photocatalytic Degradation of Pollutants. *J. Mater. Chem. A* **2014**, *2*, 5340−5351.
(82) Ye, W.; Shao, Y.; Hu, X.; Liu, C.; Sun, C. Highly Enhanced Photoreductive Degradation of Polybromodiphenyl Ethers with g-C_3N_4/TiO_2 under Visible Light Irradiation. *Nanomaterials* **2017**, 76.
(83) Bae, E.; Choi, W. Highly Enhanced Photoreductive Degradation of Perchlorinated Compounds on Dye-Sensitized Metal/TiO_2 Under Visible Light. *Environ. Sci. Technol.* **2003**, *37*, 147−152.
(84) Tugaoen, H. O.; Garciasegura, S.; Hristovski, K.; Westerhoff, P. Challenges in Photocatalytic Reduction of Nitrate as a Water Treatment Technology. *Sci. Total Environ.* **2017**, *599−600*, 1524−1551.
(85) Kamegawa, T.; Seto, H.; Matsuura, S.; Yamashita, H. Preparation of Hydroxynaphthalene-Modified TiO_2 via Formation of Surface Complexes and Their Applications in the Photocatalytic Reduction of Nitrobenzene Under Visible-Light Irradiation. *ACS Appl. Mater. Interfaces* **2012**, *4*, 6635−6639.
(86) Toyao, T.; Saito, M.; Yu, H.; Mochizuki, K.; Iwata, M.; Higashimura, H.; Matsuoka, M. Efficient Hydrogen Production and Photocatalytic Reduction of Nitrobenzene over a Visible-Light-Responsive Metal−Organic Framework Photocatalyst. *Catal. Sci. Technol.* **2013**, *3*, 2092−2097.
(87) Dai, X.; Xie, M.; Meng, S.; Fu, X.; Chen, S. Coupled Systems For Selective Oxidation of Aromatic Alcohols to Aldehydes and Reduction of Nitrobenzene into Aniline Using CdS/g-C_3N_4 Photocatalyst Under Visible Light Irradiation. *Appl. Catal., B* **2014**, *158−159*, 382−390.
(88) Yang, Z.; Xu, X.; Liang, X.; Lei, C.; Cui, Y.; Wu, W.; Yang, Y.; Zhang, Z.; Lei, Z. Construction of Heterostructured MIL-125/Ag/g-C_3N_4 Nanocomposite as an Efficient Bifunctional Visible Light Photocatalyst for the Organic Oxidation and Reduction Reactions. *Appl. Catal., B* **2017**, *205*, 42−54.
(89) Zhang, L.; He, X.; Xu, X.; Liu, C.; Duan, Y.; Hou, L.; Zhou, Q.; Ma, C.; Yang, X.; Liu, R.; et al. Highly Active TiO_2/g-C_3N_4/G Photocatalyst with Extended Spectral Response towards Selective Reduction of Nitrobenzene. *Appl. Catal., B* **2017**, *203*, 1−8.
(90) Huang, D.; Gong, X.; Liu, Y.; Zeng, G.; Lai, C.; Bashir, H.; Zhou, L.; Wang, D.; Xu, P.; Cheng, M.; Wan, J. Effects of Calcium at Toxic Concentrations of Cadmium in Plants. *Planta* **2017**, *245*, 863−873.
(91) Huang, D.; Liu, L.; Zeng, G.; Xu, P.; Chao, H.; Deng, L.; Wang, R.; Jia, W. The Effects of Rice Straw Biochar on Indigenous Microbial Community and Enzymes Activity in Heavy Metal-Contaminated Sediment. *Chemosphere* **2017**, *174*, 545−553.
(92) Huang, D.; Deng, R.; Wan, J.; Zeng, G.; Xue, W.; Wen, X.; Zhou, C.; Hu, L.; Liu, X.; Xu, P.; et al. Remediation of Lead-Contaminated Sediment by Biochar-Supported Nano-Chlorapatite: Accompanied with the Change of Available Phosphorus and Organic Matters. *J. Hazard. Mater.* **2018**, *348*, 109−116.
(93) Gong, X.; Huang, D.; Liu, Y.; Zeng, G.; Wang, R.; Wan, J.; Zhang, C.; Cheng, M.; Qin, X.; Xue, W. Stabilized Nanoscale Zero-Valent Iron Mediated Cadmium Accumulation and Oxidative Damage of *Boehmeria nivea* (L.) Gaudich Cultivated in Cadmium Contaminated Sediments. *Environ. Sci. Technol.* **2017**, *51*, 11308−11316.
(94) Huang, D.; Xue, W.; Zeng, G.; Wan, J.; Chen, G.; Huang, C.; Zhang, C.; Cheng, M.; Xu, P. Immobilization of Cd in River Sediments by Sodium Alginate Modified Nanoscale Zero-Valent Iron: Impact on Enzyme Activities and Microbial Community Diversity. *Water Res.* **2016**, *106*, 15−25.
(95) Sahinkaya, E.; Kilic, A. Heterotrophic and Elemental-Sulfur-Based Autotrophic Denitrification Processes for Simultaneous Nitrate and Cr(VI) Reduction. *Water Res.* **2014**, *50*, 278−286.
(96) Huang, D.; Guo, X.; Peng, Z.; Zeng, G.; Xu, P.; Gong, X.; Deng, R.; Xue, W.; Wang, R.; Yi, H.; Liu, C. White Rot Fungi and Advanced Combined Biotechnology with Nanomaterials: Promising Tools for Endocrine-Disrupting Compounds Biotransformation. *Crit. Rev. Biotechnol.* **2017**, 679−689.
(97) Huang, D. L.; Zeng, G. M.; Feng, C. L.; Hu, S.; Jiang, X. Y.; Tang, L.; Su, F. F.; Zhang, Y.; Zeng, W.; Liu, H. L. Degradation of Lead-Contaminated Lignocellulosic Waste by Phanerochaete Chrysosporium and the Reduction of Lead Toxicity. *Environ. Sci. Technol.* **2008**, *42*, 4946−4951.
(98) Xue, W.; Huang, D.; Zeng, G.; Wan, J.; Zhang, C.; Xu, R.; Cheng, M.; Deng, R. Nanoscale Zero-Valent Iron Coated with Rhamnolipid as an Effective Stabilizer for Immobilization of Cd and Pb in River Sediments. *J. Hazard. Mater.* **2018**, *341*, 381−389.
(99) Gong, X.; Huang, D.; Liu, Y.; Zeng, G.; Wang, R.; Wei, J.; Huang, C.; Xu, P.; Wan, J.; Zhang, C. Pyrolysis and Reutilization of Plant Residues after Phytoremediation of Heavy Metals Contaminated Sediments: For Heavy Metals Stabilization and Dye Adsorption. *Bioresour. Technol.* **2018**, *253*, 64−71.
(100) Li, N.; Tian, Y.; Zhao, J.; Zhang, J.; Zhang, J.; Zuo, W.; Ding, Y. Efficient Removal of Chromium from Water by Mn_3O_4@ZnO/Mn_3O_4 Composite Under Simulated Sunlight Irradiation: Synergy of Photocatalytic Reduction and Adsorption. *Appl. Catal., B* **2017**, *214*, 126−136.
(101) Li, Y.; Bian, Y.; Qin, H.; Zhang, Y.; Bian, Z. Photocatalytic Reduction Behavior of Hexavalent Chromium on Hydroxyl Modified Titanium Dioxide. *Appl. Catal., B* **2017**, *206*, 293−299.
(102) Pope, C. N. Organophosphorus Pesticides: Do They All Have the Same Mechanism of Toxicity? *J. Toxicol. Environ. Health, Part B* **1999**, *2*, 161−181.
(103) Zhang, Y.; Liu, Y.; Ji, X.; Banks, C. E.; Zhang, W. Conversion of Natural Egg-Shell to 3D Flower-Like Hydroxyapatite Agglomerates for Highly Sensitive Detection of As^{3+} Ions. *Mater. Lett.* **2012**, *78*, 120−123.

DOI: 10.1021/acsami.8b03620
ACS Appl. Mater. Interfaces 2018, 10, 21035−21055

(104) Zang, Y.; Li, L.; Xu, Y.; Zuo, Y.; Li, G. Hybridization of Brookite TiO_2 with g-C_3N_4: A Visible-Light-Driven Photocatalyst for As^{3+} Oxidation, MO Degradation and Water Splitting for Hydrogen evolution. *J. Mater. Chem. A* **2014**, *2*, 15774−15780.

(105) Sridharan, K.; Jang, E.; Park, T. J. Novel Visible Light Active Graphitic C_3N_4−TiO_2 Composite Photocatalyst: Synergistic Synthesis, Growth and Photocatalytic Treatment of Hazardous Pollutants. *Appl. Catal., B* **2013**, *142−143*, 718−728.

(106) Xin, X.; Lang, J.; Wang, T.; Su, Y.; Zhao, Y.; Wang, X. Construction of Novel Ternary Component Photocatalyst $Sr_{0.25}H_{1.5}Ta_2O_6{\cdot}H_2O$ Coupled with g-C_3N_4 and Ag toward Efficient Visible Light Photocatalytic Activity for Environmental Remediation. *Appl. Catal., B* **2016**, *181*, 197−209.

(107) Sun, S.; Ji, C.; Wu, L.; Chi, S.; Qu, R.; Li, Y.; Lu, Y.; Sun, C.; Xue, Z. Facile One-Pot Construction of α-Fe_2O_3/g-C_3N_4 Heterojunction for Arsenic Removal by Synchronous Visible Light Catalysis Oxidation and Adsorption. *Mater. Chem. Phys.* **2017**, *194*, 1−8.

(108) Sun, B.; Horvat, J.; Kim, H.; Kim, W.; Ahn, J.; Wang, G. Synthesis Of Mesoporous Alpha-Fe_2O_3 Nanostructures For Highly Sensitive Gas Sensors And High Capacity Anode Materials In Lithium Ion Batteries. *J. Phys. Chem. C* **2010**, 18753−18761.

(109) Liga, M. V.; Bryant, E. L.; Colvin, V. L.; Li, Q. Virus Inactivation by Silver Doped Titanium Dioxide Nanoparticles for Drinking Water Treatment. *Water Res.* **2011**, *45*, 535−544.

(110) Li, Y.; Zhang, C.; Shuai, D.; Naraginti, S.; Wang, D.; Zhang, W. Visible-Light-Driven Photocatalytic Inactivation of MS_2 by Metal-Free g-C_3N_4: Virucidal Performance and Mechanism. *Water Res.* **2016**, *106*, 249−258.

(111) Chong, M. N.; Jin, B.; Chow, C. W. K.; Saint, C. Recent Developments in Photocatalytic Water Treatment Technology: A Review. *Water Res.* **2010**, *44*, 2997−3027.

(112) Xia, D.; Wang, W.; Yin, R.; Jiang, Z.; An, T.; Li, G.; Zhao, H.; Wong, P. K. Enhanced Photocatalytic Inactivation of *Escherichia coli* by a Novel Z-scheme g-C_3N_4/m-Bi_2O_4 Hybrid Photocatalyst Under Visible Light: The Role of Reactive Oxygen Species. *Appl. Catal., B* **2017**, *214*, 23−33.

(113) Wang, W.; Yu, J. C.; Xia, D.; Wong, P. K.; Li, Y. Graphene and g-C_3N_4 Nanosheets Cowrapped Elemental α-Sulfur As a Novel Metal-Free Heterojunction Photocatalyst for Bacterial Inactivation under Visible-Light. *Environ. Sci. Technol.* **2013**, *47*, 8724−8732.

(114) Quanjun, X.; Jiaguo, Y.; Mietek, J. Graphene-based Semiconductor Photocatalysts. *Chem. Soc. Rev.* **2012**, *41*, 782−796.

(115) Yang, Y.; Zhang, C.; Lai, C.; Zeng, G.; Huang, D.; Cheng, M.; Wang, J.; Chen, F.; Zhou, C.; Xiong, W. BiOX (X = Cl, Br, I) Photocatalytic Nanomaterials: Applications for Fuels and Environmental Management. *Adv. Colloid Interface Sci.* **2018**, 76−93.

(116) Turner, J. A. A Realizable Renewable Energy Future. *Science* **1999**, *285*, 687−689.

(117) Xie, G.; Zhang, K.; Guo, B.; Liu, Q.; Fang, L.; Gong, J. R. Graphene-Based Materials for Hydrogen Generation from Light-Driven Water Splitting †. *Adv. Mater.* **2013**, *25*, 3820−3839.

(118) Hong, Y.; Fang, Z.; Yin, B.; Luo, B.; Zhao, Y.; Shi, W.; Li, C. A Visible-Light-Driven Heterojunction for Enhanced Photocatalytic Water Splitting over Ta_2O_5 Modified g-C_3N_4 Photocatalyst. *Int. J. Hydrogen Energy* **2017**, *42*, 6738−6745.

(119) Wang, B.; Zhang, J.; Huang, F. Enhanced Visible Light Photocatalytic H_2 Evolution of Metal-Free g-C_3N_4/SiC Heterostructured Photocatalysts. *Appl. Surf. Sci.* **2017**, *391*, 449−456.

(120) Li, J.; Yin, Y.; Liu, E.; Ma, Y.; Wan, J.; Fan, J.; Hu, X. In Situ Growing Bi_2MoO_6 on g-C_3N_4 Nanosheets with Enhanced Photocatalytic Hydrogen Evolution and Disinfection of Bacteria Under Visible Light Irradiation. *J. Hazard. Mater.* **2017**, *321*, 183−192.

(121) Ye, R.; Fang, H.; Zheng, Y. Z.; Li, N.; Wang, Y.; Tao, X. Fabrication of $CoTiO_3$/g-C_3N_4 Hybrid Photocatalysts with Enhanced H_2 Evolution: Z-Scheme Photocatalytic Mechanism Insight. *ACS Appl. Mater. Interfaces* **2016**, *8*, 13879−13889.

(122) Akple, M. S.; Low, J.; Wageh, S.; Al-Ghamdi, A. A.; Yu, J.; Zhang, J. Enhanced Visible Light Photocatalytic H_2-Production of g-C_3N_4/WS_2 Composite Heterostructures. *Appl. Surf. Sci.* **2015**, *358*, 196−203.

(123) Tian, Y.; Ge, L.; Wang, K.; Chai, Y. Synthesis of Novel MoS_2/g-C_3N_4 Heterojunction Photocatalysts with Enhanced Hydrogen Evolution Activity. *Mater. Charact.* **2014**, *87*, 70−73.

(124) Ji, C.; Yin, S.-N.; Sun, S.; Yang, S. An in Situ Mediator-Free Route to Fabricate Cu_2O/g-C_3N_4 Type-II Heterojunctions for Enhanced Visible-Light Photocatalytic H_2 Generation. *Appl. Surf. Sci.* **2018**, *434*, 1224−1231.

(125) Yan, M.; Hua, Y.; Zhu, F.; Sun, L.; Gu, W.; Shi, W. Constructing Nitrogen Doped Graphene Quantum Dots-$ZnNb_2O_6$/g-C_3N_4 Catalysts for Hydrogen Production Under Visible Light. *Appl. Catal., B* **2017**, *206*, 531−537.

(126) Song, C.; Fan, M.; Shi, W.; Wang, W. High-Performance for Hydrogen Evolution and Pollutant Degradation of Reduced Graphene Oxide/Two-Phase g-C_3N_4 Heterojunction Photocatalysts. *Environ. Sci. Pollut. Res.* **2018**, *25*, 14486−14498.

(127) Liang, Q.; Jin, J.; Liu, C.; Xu, S.; Yao, C.; Li, Z. Fabrication of the Ternary Heterojunction $Cd_{0.5}Zn_{0.5}S$@UIO-66@g-C_3N_4 for Enhanced Visible-Light Photocatalytic Hydrogen Evolution and Degradation of Organic Pollutants. *Inorg. Chem. Front.* **2018**, *5*, 335−343.

(128) Wang, M.; Ju, P.; Zhao, Y.; Li, J.; Han, X.; Hao, Z. In Situ Ion Exchange Synthesis of MoS_2/g-C_3N_4 Heterojunction for Highly Efficient Hydrogen Production. *New J. Chem.* **2018**, *42*, 910−917.

(129) Wen, J.; Xie, J.; Zhang, H.; Zhang, A.; Liu, Y.; Chen, X.; Xin, L. Constructing Multi-Functional Metallic Ni Interface Layers in the g-C_3N_4 Nanosheets/Amorphous NiS Heterojunctions for Efficient Photocatalytic H_2 Generation. *ACS Appl. Mater. Interfaces* **2017**, *9*, 14031−14042.

(130) Yuan, Y. P.; Cao, S. W.; Liao, Y. S.; Yin, L. S.; Xue, C. Red Phosphor/g-C_3N_4 Heterojunction with Enhanced Photocatalytic Activities for Solar Fuels Production. *Appl. Catal., B* **2013**, *140−141*, 164−168.

(131) Zhang, J.; Wang, Y.; Jin, J.; Zhang, J.; Lin, Z.; Huang, F.; Yu, J. Efficient Visible-Light Photocatalytic Hydrogen Evolution and Enhanced Photostability of Core/Shell CdS/g-C_3N_4 Nanowires. *ACS Appl. Mater. Interfaces* **2013**, *5*, 10317−10324.

(132) Chen, Z.; Sun, P.; Fan, B.; Zhang, Z.; Fang, X. In Situ Template-Free Ion-Exchange Process to Prepare Visible-Light-Active g-C_3N_4/NiS Hybrid Photocatalysts with Enhanced Hydrogen Evolution Activity. *J. Phys. Chem. C* **2014**, *118*, 7801−7807.

(133) Zhao, G.; Huang, X.; Fina, F.; Zhang, G.; Irvine, J. T. S. Facile Structure Design Based on C_3N_4 for Mediator-free Z-Scheme Water Splitting Under Visible Light. *Catal. Sci. Technol.* **2015**, *5*, 3416−3422.

(134) Jiang, D.; Li, J.; Xing, C.; Zhang, Z.; Meng, S.; Chen, M. Two-Dimensional $CaIn_2S_4$/g-C_3N_4 Heterojunction Nanocomposite with Enhanced Visible-Light Photocatalytic Activities: Interfacial Engineering and Mechanism Insight. *ACS Appl. Mater. Interfaces* **2015**, *7*, 19234−19242.

(135) Mao, Z.; Chen, J.; Yang, Y.; Wang, D.; Bie, L. J.; Fahlman, B. D. Novel g-C_3N_4/CoO Nanocomposites with Significantly Enhanced Visible-Light Photocatalytic Activity for H_2 Evolution. *ACS Appl. Mater. Interfaces* **2017**, *9*, 12427−12435.

(136) Cox, P. M.; Betts, R. A.; Jones, C. D.; Spall, S. A.; Totterdell, I. J. Acceleration of Global Warming Due to Carbon-Cycle Feedbacks in a Coupled Climate Model. *Nature* **2000**, *408*, 184−187.

(137) Le Quéré, C.; Raupach, M. R.; Canadell, J. G.; Marland, G.; et al. Trends in the Sources and Sinks of Carbon Dioxide. *Nat. Geosci.* **2009**, *2*, 831−836.

(138) Wang, M.; Shen, M.; Zhang, L.; Tian, J.; Jin, X.; Zhou, Y.; Shi, J. 2D-2D MnO_2/g-C_3N_4 Heterojunction Photocatalyst: In-Situ Synthesis and Enhanced CO_2 Reduction Activity. *Carbon* **2017**, *120*, 23−31.

(139) Ong, W. J.; Tan, L. L.; Chai, S. P.; Yong, S. T. Heterojunction Engineering of Graphitic Carbon Nitride (g-C_3N_4) via Pt Loading with Improved Daylight-Induced Photocatalytic Reduction of Carbon Dioxide to Methane. *Dalton Trans.* **2015**, *44*, 1249−1257.

DOI: 10.1021/acsami.8b03620
ACS Appl. Mater. Interfaces 2018, 10, 21035−21055

(140) Hou, J.; Cao, S.; Wu, Y.; Liang, F.; Sun, Y.; Lin, Z.; Sun, L. Simultaneously Efficient Light Absorption and Charge Transport of Phosphate and Oxygen-Vacancy Confined in Bismuth Tungstate Atomic Layers Triggering Robust Solar CO_2 Reduction. *Nano Energy* **2017**, *32*, 359−366.
(141) Mao, J.; Li, K.; Peng, T. Recent Advances in the Photocatalytic CO_2 Reduction over Semiconductors. *Catal. Sci. Technol.* **2013**, *3*, 2481−2498.
(142) Bai, Y.; Ye, L.; Wang, L.; Shi, X.; Wang, P.; Bai, W.; Wong, P. K. g-C_3N_4/$Bi_4O_5I_2$ Heterojunction with I^{3-}/I^- Redox Mediator for Enhanced Photocatalytic CO_2 Conversion. *Appl. Catal., B* **2016**, *194*, 98−104.
(143) Di, T.; Zhu, B.; Cheng, B.; Yu, J.; Xu, J. A Direct Z-scheme g-C_3N_4/SnS_2 Photocatalyst with Superior Visible-Light CO_2 Reduction Performance. *J. Catal.* **2017**, *352*, 532−541.
(144) Tonda, S.; Kumar, S.; Bhardwaj, M.; Yadav, P.; Ogale, S. g-C_3N_4/NiAl-LDH 2D/2D Hybrid Heterojunction for High-Performance Photocatalytic Reduction of CO_2 into Renewable Fuels. *ACS Appl. Mater. Interfaces* **2018**, *10*, 2667−2678.
(145) Jiang, Z.; Wan, W.; Li, H.; Yuan, S.; Zhao, H.; Wong, P. K. A Hierarchical Z-Scheme α-Fe_2O_3/g-C_3N_4 Hybrid for Enhanced Photocatalytic CO_2 Reduction. *Adv. Mater.* **2018**, No. 1706108.
(146) Zhou, S.; Liu, Y.; Li, J.; Wang, Y.; Jiang, G.; Zhao, Z.; Wang, D.; Duan, A.; Liu, J.; Wei, Y. Facile In Situ Synthesis of Graphitic Carbon Nitride (g-C_3N_4)-N-TiO_2 Heterojunction as an Efficient Photocatalyst for the Selective Photoreduction of CO_2 to CO. *Appl. Catal., B* **2014**, *158−159*, 20−29.
(147) Li, M.; Zhang, L.; Fan, X.; Zhou, Y.; Wu, M.; Shi, J. Highly Selective CO_2 Photoreduction to CO over g-C_3N_4/Bi_2WO_6 Composites Under Visible Light. *J. Mater. Chem. A* **2015**, *3*, 5189−5196.
(148) Wang, J.-C.; Yao, H.-C.; Fan, Z.-Y.; Zhang, L.; Wang, J.-S.; Zang, S.-Q.; Li, Z.-J. Indirect Z-scheme BiOI/g-C_3N_4 Photocatalysts with Enhanced Photoreduction CO_2 Activity under Visible Light Irradiation. *ACS Appl. Mater. Interfaces* **2016**, *8*, 3765−3775.
(149) He, Y.; Zhang, L.; Fan, M.; Wang, X.; Walbridge, M. L.; Nong, Q.; Wu, Y.; Zhao, L. Z-scheme SnO_{2-x}/g-C_3N_4 Composite as an Efficient Photocatalyst for Dye Degradation and Photocatalytic CO_2 Reduction. *Sol. Energy Mater. Sol. C* **2015**, *137*, 175−184.
(150) Ohno, T.; Murakami, N.; Koyanagi, T.; Yang, Y. Photocatalytic Reduction of CO_2 over a Hybrid Photocatalyst Composed of WO_3 and Graphitic Carbon Nitride (g-C_3N_4) Under Visible Light. *J. CO_2 Util.* **2014**, *6*, 17−25.
(151) Yu, W.; Xu, D.; Peng, T. Enhanced Photocatalytic Activity of g-C_3N_4 for Selective CO_2 Reduction to CH_3OH via Facile Coupling of ZnO: A Direct Z-scheme Mechanism. *J. Mater. Chem. A* **2015**, *3*, 19936−19947.
(152) Zhou, J.; Chen, W.; Sun, C.; Han, L.; Qin, C.; Chen, M.; Wang, X.; Wang, E.; Su, Z. Oxidative Polyoxometalates Modified Graphitic Carbon Nitride for Visible-Light CO_2 Reduction. *ACS Appl. Mater. Interfaces* **2017**, *9*, 11689−11695.
(153) Liu, Y.; Ma, H.; Zhang, Y.; Pang, X.; Fan, D.; Wu, D.; Wei, Q. Visible Light Photoelectrochemical Aptasensor for Adenosine Detection Based on CdS/PPy/g-C_3N_4 Nanocomposites. *Biosens. Bioelectron.* **2016**, *86*, 439−445.
(154) Huang, D. W.; Niu, C. G.; Zeng, G. M.; Ruan, M. Time-Resolved Fluorescence Biosensor for Adenosine Detection Based on Home-Made Europium Complexes. *Biosens. Bioelectron.* **2011**, *29*, 178−183.
(155) Cai, S.; Sun, Y.; Lau, C.; Lu, J. Sensitive Chemiluminescence Aptasensor Based on Exonuclease-Assisted Recycling Amplification. *Anal. Chim. Acta* **2013**, *761*, 137−142.
(156) Liu, Z. F.; Ge, J.; Zhao, X. S. Quantitative Detection of Adenosine in Urine Using Silver Enhancement of Aptamer-Gold Nanoparticle Aggregation and Progressive Dilution. *Chem. Commun.* **2011**, *47*, 4956−4958.
(157) Meyer, K. D.; Jaffrey, S. R. The Dynamic Epitranscriptome: N^6-Methyladenosine and Gene Expression Control. *Nat. Rev. Mol. Cell Biol.* **2014**, *15*, 313−326.
(158) Wang, H.; Zhang, Q.; Yin, H.; Wang, M.; Jiang, W.; Ai, S. Photoelectrochemical Immunosensor for Methylated RNA Detection Based on g-C_3N_4/CdS Quantum Dots Heterojunction and Phos-Tag-Biotin. *Biosens. Bioelectron.* **2017**, *95*, 124−130.
(159) Shafiee, S.; Topal, E. When Will Fossil Fuel Reserves be Diminished? *Energy Policy* **2009**, *37*, 181−189.
(160) Lewis, N. S. Toward Cost-Effective Solar Energy Use. *Science* **2007**, *315*, 798−801.
(161) Ahmad, M. S.; Pandey, A. K.; Rahim, N. A. Advancements in the Development of TiO_2 Photoanodes and Its Fabrication Methods for Dye Sensitized Solar Cell (DSSC) Applications. A Review. *Renewable Sustainable Energy Rev.* **2017**, *77*, 89−108.
(162) Xu, J.; Wang, G.; Fan, J.; Liu, B.; Cao, S.; Yu, J. g-C_3N_4 Modified TiO_2 Nanosheets with Enhanced Photoelectric Conversion Efficiency in Dye-Sensitized Solar Cells. *J. Power Sources* **2015**, *274*, 77−84.
(163) Ansari, M. S.; Banik, A.; Qureshi, M. Morphological Tuning of Photo-booster g-C_3N_4 with Higher Surface Area and Better Charge Transfers for Enhanced Power Conversion Efficiency of Quantum Dot Sensitized Solar Cells. *Carbon* **2017**, *121*, 90−105.
(164) Yuan, Z.; Tang, R.; Zhang, Y.; Yin, L. Enhanced Photovoltaic Performance of Dye-Sensitized Solar Cells Based on Co_9S_8 Nanotube Array Counter Electrode and TiO_2/g-C_3N_4 Heterostructure Nanosheet Photoanode. *J. Alloys Compd.* **2017**, *691*, 983−991.
(165) Xiao, J.; Han, Q.; Xie, Y.; Yang, J.; Su, Q.; Chen, Y.; Cao, H. Is C_3N_4 Chemically Stable towards Reactive Oxygen Species in Sunlight-Driven Water Treatment? *Environ. Sci. Technol.* **2017**, *51*, 13380−13387.

DOI: 10.1021/acsami.8b03620
ACS Appl. Mater. Interfaces 2018, 10, 21035−21055